Magnetic fabric and archaeomagnetic analyses of anthropogenic ash horizons in a cave sediment succession (Crvena Stijena site, Montenegro)

Balázs Bradák,[1] Ángel Carrancho,[2] Ángela Herrejón Lagunilla,[1] Juan J. Villalaín,[1] Gilliane F. Monnier,[3] Gilbert Tostevin,[3] Carolina Mallol,[4,5] Goran Pajović,[6] Mile Baković[7] and Nikola Borovinić[7]

[1]*Laboratorio de Paleomagnetismo, Departamento de Física, Universidad de Burgos, Av. Cantabria s/n, Burgos, Spain, 09006. E-mail:* bradak.b@gmail.com
[2]*Área de Prehistoria, Departamento de Historia, Geografía y Comunicación, Universidad de Burgos, Edificio I+D+I, Plaza Misael Bañuelos s/n, Burgos 09001, Spain*
[3]*Department of Anthropology, University of Minnesota Twin Cities, 395 Humphrey Center, 30119th Ave S, Minneapolis, MN 55455, United States*
[4]*Departamento de Geografía e Historia, Área de Prehistoria (Facultad de Humanidades), Universidad de La Laguna, Campus de Guajara, La Laguna, Tenerife, Spain, Av. Astrofísico Francisco Sánchez 2, La Laguna 38206, Spain*
[5]*Archaeological Micromorphology and Biomarker Research Lab, Instituto Universitario de Bio-Orgánica Antonio González, La Laguna, Tenerife, Spain*
[6]*National Museum of Montenegro, Novice Cerovida bb., Cetinje 81.250, Montenegro*
[7]*Center for Conservation and Archaeology of Montenegro, UI. Njegoseva bb., Cetinje, Montenegro*

SUMMARY
An archaeomagnetic, rock magnetic and magnetic fabric study has been carried out on seven anthropogenic ash horizons in the Middle Palaeolithic sedimentary level XXIV at the rock shelter of Crvena Stijena ('Red Rock'), Montenegro. The study has multiple goals, including the identification of iron bearing minerals formed during combustion, assessment of the suitability of these combustion features for recording the Earth´s magnetic field direction, revelation of the magnetic fabric and its significance in the characterization of cave (rock shelter) burnt facies, and identification of post-burning alteration processes. Magnetite has been identified as the main ferromagnetic component of the ash. The ash layers exhibit a high thermomagnetic reversibility in contrast to the irreversible behaviour of their subjacent burnt black layers which is related to the different temperatures attained. Seven mean archaeomagnetic directions were obtained with acceptable statistical values indicating that these features recorded the field direction at the time of burning. However, some of them are out of the expected range of secular variation for mid-latitude regions suggesting post-burning alterations. The magnetic fabric of the ash was characterized by anisotropy of low field magnetic susceptibility measurements. Statistical analysis (box and whisker plot) of the basic anisotropy parameters, such as foliation, lineation, degree of anisotropy and the shape parameter, along with the alignment of the principal susceptibilities on stereoplots, revealed variation among the ash units. The diverse, oblate to prolate, lineated or strongly foliated, quasi-horizontally and vertically oriented fabrics of the units may indicate different slope processes, such as orientation by gravity, solifluction, run-off water, quasi-vertical migration of groundwater and post-burning/post-depositional alteration of the fabric by rockfall impact. In sum, the magnetic characterization of the ash layers has shown the occurrence of different post-burning alteration processes previously not identified at the site. Alteration processes in prehistoric combustion features are often identified from macroscopic observations but our study demonstrates that multiple processes can affect them and are usually unnoted because they take place on a microscopic scale. Their identification is critical for a correct chronological and cultural interpretation of a site (e.g. collection of samples for dating, stratigraphic displacement of remains), especially if significant alterations are involved. Magnetic methods are therefore a powerful but underutilized tool in palaeolithic research for the identification and evaluation of taphonomic processes affecting prehistoric fires.

1 INTRODUCTION

Archaeological and palaeoanthropological remains contained in the stratified sequences of many caves and rock shelters contain a wealth of information for reconstructing human evolution (Schwarcz & Rink 2001). Among the different types of sediments that may appear in prehistoric cave sequences, burnt facies represent a unique group as they are generally related to anthropogenic activities (Mentzer 2014; Mallol *et al.* 2017). This is particularly true for Middle Palaeolithic (*ca.* 250–40 ky BP) sites where different activities such as stone tool knapping, butchering and even sleeping have been associated with combustion structures (Vaquero & Pastó 2001; Vallverdú *et al.* 2012; Machado *et al.* 2013; Mallol *et al.* 2019). Well preserved Middle Palaeolithic combustion structures are mainly composed of a white and/or grey ash layer over a subjacent black layer and/or rubefacted facies (e.g. Mentzer 2014; Goldberg *et al.* 2017; Mallol & Henry 2017; Mallol *et al.* 2017). However, their preservation is variable, and their identification is not always straightforward as different taphonomic and post-depositional processes (e.g. bioturbation, diagenesis, etc.) can substantially alter them, compromising the integrity of the cultural record. The identification of these processes has been the subject of numerous studies over the years; many methods have been deployed to understand archaeological site formation processes in rock shelters and caves, especially micromorphological and mineralogical (Schiegl *et al.* 1996; Karkanas *et al.* 2000; Weiner *et al.* 2002; Weiner 2010; Aldeias *et al.* 2012; Mallol *et al.* 2013; Shahack-Gross *et al.* 2014; Monnier 2018). However, relatively few magnetic techniques have been applied until recently.

Within the last few years, magnetic methods such as archaeomagnetism and rock-magnetism have begun to be applied to palaeolithic sites with evidence of fire. Ferromagnetic minerals— mainly iron oxides and hydroxides—have very sensitive magnetic properties easily transformed by heating. Following heating over 500–600 °C, ferromagnetic (*s.l.*) minerals may acquire a strong and stable remanent magnetization (thermal remanent magnetization or TRM) parallel to the ambient Earth's magnetic field during cooling (e.g. Tauxe 2010). If the combustion structure is *in situ* (it preserves its position as it was last heated), it may potentially be used for archaeomagnetic dating purposes as long as secular variation (SV) records or geomagnetic field models exist for the region and period of interest (Morales *et al.* 2015; Carrancho *et al.* 2016a; Peters *et al.* 2018; García-Redondo *et al.* 2019; Gómez-Paccard *et al.* 2019). The absence of such geomagnetic records for chronologies prior to the last 3–4 millennia (e.g. Goguitchaisvili *et al.* 2018; Molina-Cardín *et al.* 2018) hampers the application of archeomagnetic dating to Palaeolithic sites. Nonetheless, archaeomagnetic and rock-magnetic studies have recently successfully been applied in Middle Palaeolithic sites to identify human occupations in palimpsests contexts (e.g. Carrancho *et al.* 2016a; Zeigen *et al.* 2019) or to reconstruct burning conditions in hearths (e.g. Jrad *et al.* 2014; Aldeias 2017).

Anisotropy of low field magnetic susceptibility (AMS) is a type of magnetic analysis commonly applied in a wide suite of geological contexts but rarely used in prehistoric archaeological sites. Some of its main applications consist of verifying quasi-horizontal or undisturbed states of sedimentary contexts, detecting palaeocurrents (e.g.

during water-lain sedimentation) and identifying mechanical (physical) alteration processes, which may bias palaeomagnetic results (e.g. Oliva-Urcia *et al.* 2014; Bondar & Ridush 2015; Bella *et al.* 2019). AMS is therefore an interesting but underutilized tool for reconstructing site formation processes in Palaeolithic cave sequences to assess the preservation state of the archaeological record. Along the naturally deposited sediments, it also can be used to characterize anthropogenic materials, for example ash horizons of combustion sites, appearing in cave sequence.

Ashes from Palaeolithic fires are especially interesting, as they contain neoformed ferrimagnetic minerals originating from the combustion of organic materials such as wood, bone or dung (Carrancho *et al.* 2009; Herries 2009; Jrad *et al.* 2014; Jordanova *et al.* 2019). These minerals not only generate a distinguishable magnetic enhancement which can be used as a proxy to identify fire (Jrad *et al.* 2014; Carrancho *et al.* 2016b and references therein), but may also preserve information about changes in the direction and/or intensity of the Earth's magnetic field in the past. Obtaining this archeological and geophysical information largely depends on the preservation states of the minerals. Processes such as reworking and redeposition of sediments, bioturbation, mineral diagenesis, roof fall episodes and cryoturbation, are commonly reported in cave deposits (e.g. Goldberg & Sherwood 2006, and references therein). However, to our knowledge, little is known about post-depositional processes in Palaeolithic anthropogenic combustion contexts from a magnetic point of view. Rock magnetic and fabric analysis are commonly used tools, which can provide information about various post-depositional processes, suggested above.

Prehistoric burnt sediments and ashes have previously been used to estimate firing temperatures (e.g. Linford & Platzman 2004; Kapper *et al.* 2014a, b; Carrancho *et al.* 2016b), to identify fuel sources (Peters *et al.* 2002; Church *et al.* 2007), and to evaluate the degree of preservation in cave fires (e.g. Carrancho *et al.* 2012, 2016b). Burnt materials such as flint artifacts or the sediments from combustion structures have been sporadically used to obtain directional and/or absolute archaeointensity data (Carrancho & Villalaín 2012; Carrancho *et al.* 2013; Kapper *et al.* 2014a, b; Zeigen *et al.* 2019). For the moment, Carrancho *et al.* (2012) and Kapper *et al.* (2014a, b) have used magnetic fabric analysis to identify post-depositional processes in archaeological cave fires. Parés *et al.* (2010, 2018) also combined AMS and palaeomagnetic methods to infer site formation processes in Pleistocene sites at Atapuerca, Spain, but this was not related to burnt facies. How the magnetic signature in Middle Palaeolithic combustion features is formed and preserved still remains an issue not yet studied in detail. The elaborated rock magnetic and magnetic fabric analysis in the current study, may be able to reveal additional information about the forming and preservation of magnetic components in combustion features.

The aims of this study are to evaluate the potential of the ashy layers of archaeological combustion features to reconstruct magnetic minerals and magnetic fabric forming during burning, assess their suitability to record the Earth's magnetic field direction and to identify syn/post-burning processes (e.g. compaction, erosion and reworking). The magnetic characteristics of this type of Palaeolithic combustion features (ash horizons) may provide novel and useful information to archaeologists about the formation and alteration of pyrogenic anthropogenic ash.
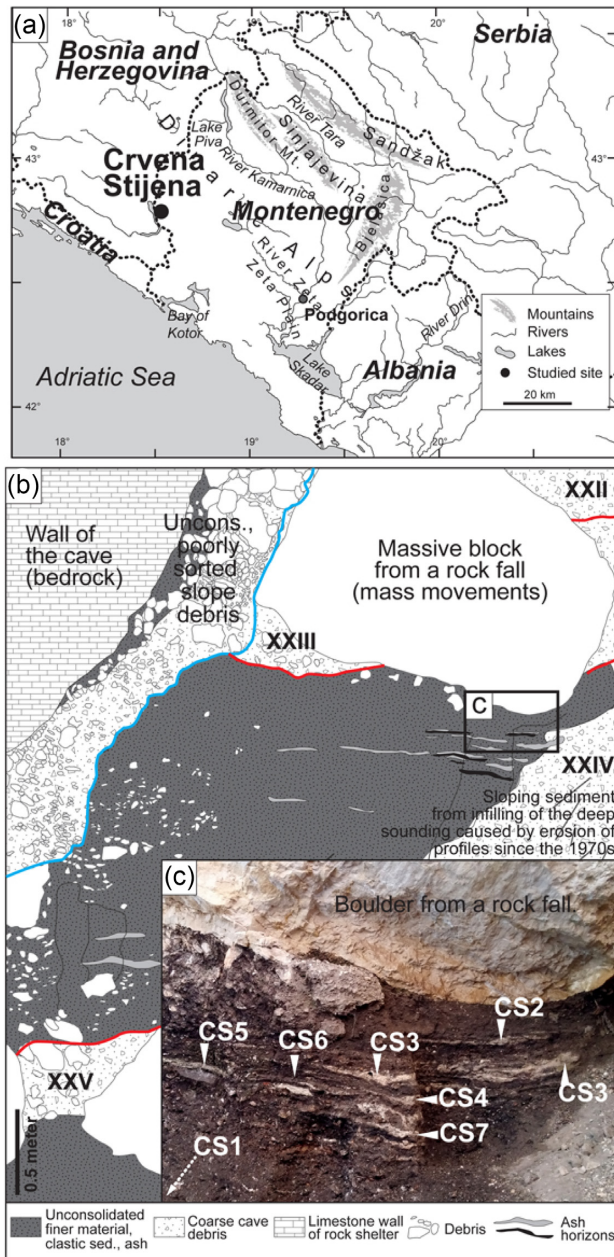
Figure 1. The locality of the studied profile (a) and the studied profile (b) with the sampled ash horizons (c). The solid red lines indicate the boundaries between unit XXII, XXIII, XXIV and XXV. The solid blue line marks the edge of the slope debris.

2 SITE AND SAMPLING

The rock shelter of Crvena Stijena in Montenegro is one of the longest and best-preserved Middle Palaeolithic (MP) sequences in southeastern Europe. Crvena Stijena (meaning 'Red Rock') is situated in a limestone cliff that is part of the Dinaric Karst, at 700 m above sea level and 32 km from the present shoreline of Adriatic Sea (Fig. 1a). The shelter is large, approximately 26 m wide at the mouth, and 15 m deep from the dripline to the back of the shelter (20–25 m deep in the lower strata).

Excavations in the 1950s and 1960s uncovered a stratified sequence of archaeological layers over 20 m deep, spanning the Middle Palaeolithic through the Bronze Age (Brodar 1958, 1958–59, 1962,

2009; Basler 1975a, b). The stratigraphy developed by geologist Brunnaker on the basis of these excavations has been recognized as still valid today by subsequent field workers (Morley 2007; Baković *et al.* 2009).

Excavations from 2004 to 2015 led by Robert Whallon (University of Michigan) and Mile Baković (Ministry of Culture of Montenegro) explored the sediments above Basler's deep sounding, uncovering in situ remains in Mesolithic and late Middle Palaeolithic sediments, as summarized in Baković *et al.* (2009) and Whallon (2017). This multidisciplinary research project also investigated the excellent preservation of fauna and combustion features at Crvena Stijena and yielded the first absolute chronology for the site, based upon an extensive radiometric dating program using TL, OSL, ESR and AMS ^{14}C methods (Mercier *et al.* 2017).

The Middle Palaeolithic layers (XII through XXXI) are capped by a thick tephra layer (layer XI), which was geochemically identified as the Y5 tephra from the Campanian Ignimbrite (CI) eruption at 39.9 ka (Morley & Woodward 2011). Faunal and taphonomic analyses have shown that hominins were by far the dominant bone accumulator in all levels and that red deer dominates the species list in all but a few of the MP layers (Morin & Soulier 2017).

Analysis of the lithic collections has shown cultural continuity throughout the Middle Palaeolithic sequence and the presence of Uluzzian elements in the uppermost MP levels, immediately below the Y-5 tephra (Mihailović *et al.* 2017). One of the most striking of the Middle Palaeolithic levels is level XXIV (the subject of the present study), a 2-m-thick level composed of layered combustion features. Lithologically, it is composed of interbedded fine sandy gravels and coarse sand with a matrix dominated by charcoal, ash, bone fragments (burnt and unburnt) and lithics (Morley 2017). The individual layers within level XXIV vary in colour and composition, from black (very rich in charcoal) to white (containing almost exclusively ash). Most layers contain very high concentrations of crushed, burnt bone. The lithic industry from this level comes from the Basler excavations, which were highly selective in what artifacts were saved; it is characterized by a diversity of raw materials, Levallois and discoidal technologies and scrapers. The scrapers are side and transversal, and some exhibit Quina or semi-Quina retouch; in addition, some are ventrally or dorsally thinned (Mihailović *et al.* 2017). The chronology of this layer is debated. Three TL dates place it in the time period of 40–85 kya (with one σ; Mercier *et al.* 2017). Taking these dates into account, the geological interpretation places level XXIV in MIS 5a. However, faunal data, which show continuity from level XXIV through XII, place the entirety of this component of the site in MIS 3 (Whallon & Morin 2017). A new excavation project resulting from a collaboration between the University of Minnesota and the National Museum of Montenegro is currently working to refine the site chronology, reconstruct site formation processes and study the anthropogenic fire record through a multidisciplinary approach.

We present a study of seven different ash lenses (CS1–CS7) sampled from the east profile of level XXIV (Figs 1b and c). 80 oriented archaeomagnetic samples were collected from these seven combustion features with an average of 8–12 samples per feature. Each one of these combustion events is composed of a white and/or grey ash facies with thicknesses ranging from 3 to 7 cm over a thin (*ca.* 0.5–2 cm) dark, charcoal-rich thermo-altered facies (hereinafter referred to as 'black layer' following Mallol *et al.* 2013). That stratigraphic arrangement (ashes-black layer couplet) corresponds to the same burning event and is usually observed both in well-preserved prehistoric combustion structures (e.g. Mentzer 2014; Mallol & Henry 2017) and experimental recreations of prehistoric fires (e.g. Mallol

et al. 2013; Herrejón-Lagunilla *et al.* 2019). The seven combustion features sampled are stratigraphically differentiated in depth within level XXIV so they were produced at different times. From top to bottom we distinguished CS2, CS3, etc., up to CS7 and at the base of the level is CS1 (Fig. 1c; Supporting Information 1). In the south side (right part) of the CS3 event, the ashes and the black layer samples are locally intermingled (sampling was avoided here for this reason). However, macroscopically, the preservation of these combustion features is good, with quite pure and well-preserved ashes occasionally including some limestone clasts of centimetre size. The lateral continuity of these combustion features varies between 0.5 and 1.5 m approximately. Sampling was performed by means of a non-magnetic cylindrical piston specially designed for soft (unlithified) lithologies with a built-in orientation system which allows a precise geographical orientation of the samples (for details, see sig. S7 of Carrancho *et al.* 2013). The device is carefully pressed against the stratigraphic profile where the combustion features are exposed. Before extracting the device from the profile, the azimuth and inclination for every sample are taken. Afterwards, the oriented samples are saved in cylindrical plastic capsules (ø 16.5 mm, length 17 mm, vol. ∼3.6 cm^3) and stored under cold conditions (∼3–4 °C) to avoid mineralogical alterations. This sampling procedure is particularly suitable for burnt facies (e.g. ashes) exposed in stratigraphic cave sections (e.g. Carrancho *et al.* 2009, 2013) and has the advantage of being little invasive obtaining one sample at each injection. Due to the thinness of the underlying black layer and to ensure that only pure burnt facies was collected avoiding mixture with unburnt sediments, samples were taken only in the ash facies. In fact, other combustion events interspersed among the 7 studied combustion features were not sampled due to their thinness. Occasionally, however, some of the ashes sampled unavoidably incorporated some sediment from the underlying black layer. One or two representative ash samples from every combustion feature ($n = 11$) were injected by the same means into quartz cylindrical capsules (3.6 cm^3) for thermal demagnetization experiments. These samples were impregnated with a solution of sodium silicate (waterglass) to consolidate them before measurement. Additionally, 11 oriented control samples of unburnt sediment from level XXIV were also collected by the same means around 10 cm below the base of the boulder. Their sampling was difficult due to the presence of many gravel-sized clasts within the sedimentary fill. Bulk (unoriented) sample was also collected from every facies to study in detail their magnetic properties.

3 METHODS

Archaeomagnetic, rock magnetic and magnetic fabric experiments were performed at the Palaeomagnetic Laboratory of the University of Burgos (Burgos, Spain). The measurement of the natural remanent magnetization (NRM) was carried out with a three-axis 2G SQUID cryogenic magnetometer. The NRM measurements were performed with the aid of a non-magnetic sample holder specifically adapted to the samples´ shape taking special care of the orientation marks. The NRM stability was analysed both by progressive alternating field (AF) and thermal demagnetization. Stepwise progressive AF demagnetization was carried out in 21 steps up to 90 mT. Thermal demagnetization was performed in 19 heating steps up to 585 °C with a TD48-SC (ASC Scientific) thermal demagnetizer. Low-field magnetic susceptibility was measured initially at room temperature with a Kappabridge KLY-4 (AGICO, Czech

Republic). Standard orthogonal NRM demagnetization plots were used to interpret the structure of remanence components and to calculate the direction of the Characteristic Remanent Magnetization (ChRM) by principal component analyses (Kirschvink 1980). Remasoft software 3.0 (Chadima & Hrouda 2006) was used to interpret the directional data. The mean archaeomagnetic direction for every combustion feature was calculated using Fisher's (1953) statistics.

To estimate the domain state of the ferromagnetic (*s.l.*) minerals, hysteresis measurements and stepwise isothermal remanent magnetization (IRM) acquisition experiments were conducted on a Variable Field Translation Balance (MMVFTB, Magnetic Instruments). A maximum applied field of 1T (the limitation of the instrument) was used during the IRM, hysteresis and backfield coercivity measurements. IRMs were measured in ∼25 steps (Supplementary Material 1). IRM data from 10 pilot samples were analysed by the quantification of magnetic coercivity components with the analysis of acquisition curves of IRM (Kruiver *et al.* 2001), which allowed us to separate various magnetic mineral populations based on their calculated mean coercivity ($B_{1/2}$) and dispersion parameter (DP) by the use of IRMUNMIX2_2 (Heslop *et al.* 2002) and the IRL CLG1 worksheet (Kruiver *et al.* 2001).

Thermomagnetic experiments (temperature dependence of the magnetization) were also executed by MMVFTB from room temperature (∼20–25 °C) up to 700 °C in air.

The dia/paramagnetic correction of the hysteresis curve, determination of Curie temperature (both from second derivative as it described in Leonhardt 2006, and following the way of Moskowitz 1981) and the results of rock magnetic measurements were obtained by RockMagAnalyzer1.1 software (Leonhardt 2006). The characteristic inflection points of the heating curves were determined by using the method of Grommé *et al.* (1969) as well.

Anisotropy of low field magnetic susceptibility (AMS) was determined by using a KLY-4S Kappabridge (AGICO) instrument. The samples were measured by using the rotator of the instrument. The susceptibility values and directions of principal axes (maximum—κ_{max}; intermediate—κ_{int} and minimum—κ_{min}) were determined by computer analysis, and numerous statistical parameters were used to characterize the magnetic fabric (MF) calculated using the principal susceptibility values (Anisoft 4.2 software; Chadima & Jelinek 2009). In the course of data verification, results with *F* statistics results: $F < 3.48$; 95 per cent significance level (Jelinek 1977) were excluded. Various AMS parameters were also examined, following the method of Lagroix & Banerjee (2004) and Zhu *et al.* (2004). The $\varepsilon12$–F12 plot was studied to identify significant lineation in the samples ($\varepsilon12 < 20$ and $F12 > 4$, Zhu *et al.* 2004). Furthermore, the relationship between foliation and F23 was also investigated (F23–F plot, Zhu *et al.* 2004) in order to reveal well-resolved magnetic foliation in the fabric ($F23 > 10$). Where the F12 and $\varepsilon12$ statistics did not show strong anisotropy, but the alignment of the principal axes, related to the same stratigraphic horizons, indicated some characteristic orientation or fabric in the stereoplots, the data from those samples were used (Supplementary Material 1).

Basic anisotropy parameters, such as lineation (*L*) and foliation (*F*), were calculated as $L = \kappa_{max}/\kappa_{int}$ and $F = \kappa_{int}/\kappa_{min}$ (Tarling & Hrouda 1993). Corrected degree of anisotropy (*Pj*) was calculated as in Jelinek (1981). Control measurements have been made on samples originated from the sediment unit located between CS2 ash horizon and a massive block from a rockfall (Fig. 1b).

4 RESULTS

4.1 Rock magnetic experiments

The coercivity ratio H_{cr}/H_c (where H_c is the coercive force and H_{cr} is the remanent coercive force) ranged from $\sim$1.7 to 2.1 for all samples. The M_{rs}/M_s ratio (where M_s is the saturation magnetization and M_{rs} is the saturation remanence) ranged from $\sim$0.11 to 0.16 overall (Fig. 2a). All of the samples fell into the PSD/mixed SD and MD/VS region of the Day plot, with 70–80 per cent MD component (Dunlop 2002). The narrower range of hysteresis parameters may indicate uniform magnetic grain size characteristics for all of the sampled ash horizons (Fig. 2a).

The studied samples reached 90 per cent magnetic saturation in the $\sim$60–70 mT field, and >95 per cent, near-saturation in the $\sim$100–150 mT field in the course of IRM acquisition experiments (Figs 2b and c), indicating that the remanent magnetization is dominated by low-coercivity minerals.

Three different magnetic mineral populations were separated by the analysis of the IRM data (Coercivity population A to C; Figs 2d and e; Table 1): Population (A) very low mean coercivity group ($B_{1/2}$ average: 12.6 mT) with narrow to broader (0.03–0.29) dispersion parameter (DP); Population (B) a population which is characterized by a broader range of low mean coercivity $B_{1/2}$: from 27.7 to 120.8 mT and DP: 0.08–0.59 and Population (C) high coercivity magnetic contributors with $B_{1/2}$ from 216.7 to 328.9 mT and DP: $\sim$0.28–0.41 (Figs 2d and e). Due to the broad range of the parameters in Population B, three subgroups were separated such as Population B1, B2 and B3. Population B1 is characterized by 27.7 mT average $B_{1/2}$ and DP between 0.18 and 0.19. DP parameters of Population B2 are more scattering (0.08–0.59) and the $B_{1/2}$ is slightly higher than Population B1 (45.2–58.6 mT). Population B3 only identified in two samples and characterized by 86.1 and 120.8 mT $B_{1/2}$ and DP parameters 0.44 and 0.49. Among the studied parameters Population B1 is the most common components (77 per cent average contribution if appears, Table 1).

Three different types of thermomagnetic curves could be identified. The most common feature among all types of the heating curve was a clear decrease at about 550–600 °C, which is the Curie temperature of magnetite or oxidized magnetite (Dunlop & Özdemir 1997). Type 1 shows reversible character and no significant inflection, except a mild one around 110 °C and an inflection point at 330 °C (Fig. 3a). The suggested $\sim$110 °C inflection turns into a very characteristic 'bump' in Type 2 of thermomagnetic curves (Fig. 3b). The bump is located between 105–112 °C and 218–245 °C, with a peak around 135–149 °C. As in Type 1, the cooling curve does not show the appearance of mineral neoformation. The heating curve of Type 3 (Fig. 3c) is very similar to the heating curve of Type 2. However, Type 3 presents a non-reversible cooling curve showing significant mineral neoformation during heating (Fig. 3c).

No significant differences were found between magnetic hysteresis and coercivity properties of sediment samples and ash horizons (Figs 2a and b). The characteristics of the thermomagnetic curves of sedimentary samples are similar to the ash samples described as Type 3 group above (Figs 3c and d).

4.2 NRM directional stability

The NRM intensities of the studied collection range between 1.92×10^{-5} and 2.52×10^{-4} Am^{2}kg^{-1}, and magnetic susceptibility varies between 4.24×10^{-7} and 5.12×10^{-6} m^{3}kg^{-1}. The Koenigsberger

(Q_n) ratio (*cf.*, Stacey 1967), a parameter commonly used in archaeomagnetic studies which quantifies the ratio between remanent and induced magnetization displays low values (between 0.49 and 2.42), although within the range of other burnt facies from prehistoric fires (e.g. Carrancho *et al.* 2009; Kapper *et al.* 2014a, b). Despite the generally low Q_n values, there are interesting differences between some combustion features, being CS7 and CS3 those concentrating most samples with the lowest values and CS1 and CS6 the highest ones (Fig. 4).

Most ashes show a rather stable behaviour during progressive demagnetization. Stepwise NRM demagnetization diagrams typically show an overprint which unblocks at 200–250 °C or at fields of 10–12 mT (Figs 5a–d). It is interpreted as a secondary viscous component and generally shows a northward direction. The characteristic remanent magnetization component is univectorially defined by thermal demagnetization between 250 and 585 °C (Figs 5a and c). The ashes demagnetized by alternating fields mostly display a well-defined and stable normal polarity magnetic component which decays in a linear trend towards the origin being almost demagnetized at 90 mT (Figs 5b and d). Median destructive fields (MDF) of the total NRM range between 8 and 12 mT for all sites. These observations are also coherent with the identification of magnetite as the main remanence carrier in the ashes. AF demagnetized samples whose remanence did not go towards the origin of the orthogonal plot were excluded. Various thermally demagnetized samples were also excluded because they broke or lost orientation during the demagnetization procedures. The mean directions obtained for every combustion feature and their corresponding statistical results are compiled in Table 2. The stereograms of Figs 6(a)–(g) illustrate the same data with the mean direction and the $\alpha 95$, semi angle of confidence of each combustion feature. Fig. 6 shows all mean directions plotted together with their respective $\alpha 95$. The direction among specimens from the same burning event is more or less reproducible with reasonably acceptable statistical values. Except one $\alpha 95$ value of 17.9° (CS7), the others are comprised between 7.1° and 11.2° and k values range from 12 to 80.

4.3 Characteristics of the magnetic fabric

Overall, the basic magnetic fabric (MF) parameters of the studied ash horizons (CS1–CS7) showed quasi uniform characteristics, along with some irregularities introduced below (Figs 7a–f). Most of the studied horizons yielded by average $\sim$700–750 $\times$ 10^{-6} SI κ_{lf} except two groups: CS1 and CS2. The former was characterized by the lowest ($\sim$500 $\times$ 10^{-6} SI), and the latter was characterized by the highest ($\sim$950 $\times$ 10^{-6} SI) average κ_{lf}. Among the studied samples, group CS6 has the best defined (Interquartile range—IQR is narrow) foliated (Fig. 7b) and most oblate MF (Fig. 7e). Similar oblate, but less foliated fabric was found in the samples of CS5 horizon, and the defined foliation plane is quasi horizontal (Figs 7b, e and f). Groups CS5, CS6, completed by CS7 are characterized by weak lineation (Fig. 7c). There were no big differences in the corrected degree of anisotropy of the studied ash horizons, except CS4 in which one sample with extreme anisotropic fabric can be observed (Fig. 7d). Among the studied ash horizons, the 'most irregular group' is CS1 in the sense of basic fabric parameters. CS1 is defined by the lowest κ_{lf} (Fig. 7a), and the MF is the less anisotropic (Fig. 7d), most prolate with very scattering character (IQR is wide, Fig. 7e) and (quasi) vertically oriented (Fig. 7f).

Most of the samples from any studied horizon are represented by $\varepsilon 12 < 20$, F12 > 4 (Fig. 8a) and F23 > 10 values (Fig. 8b),
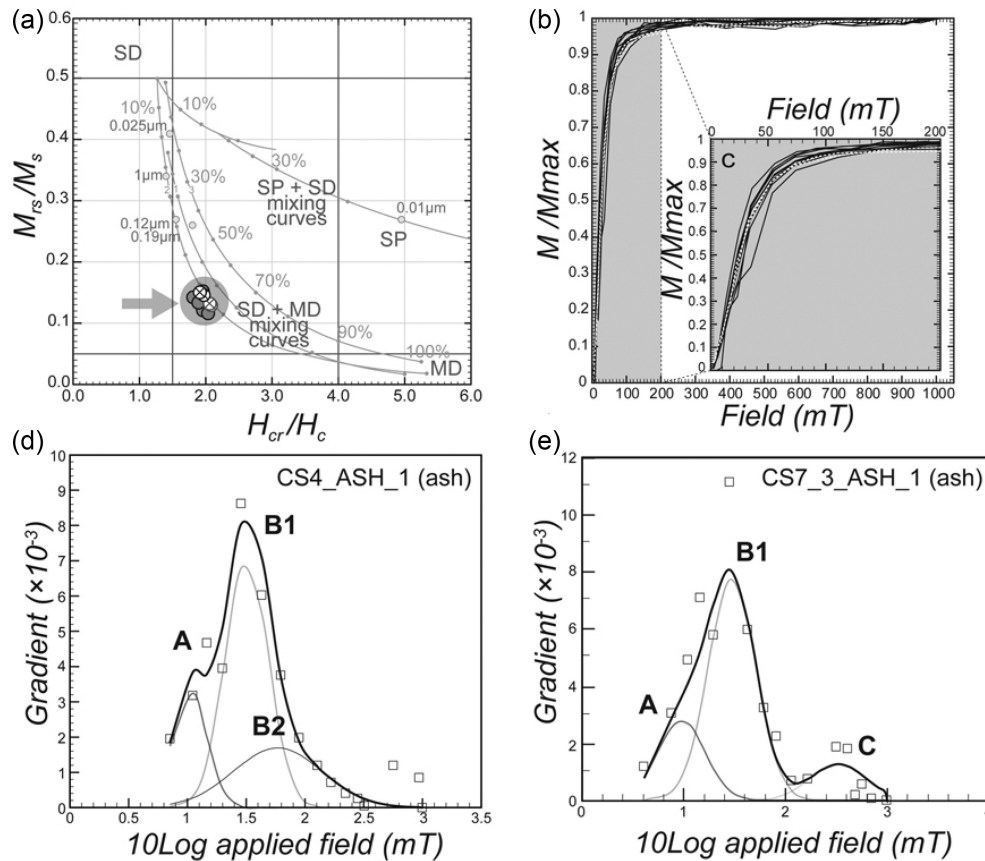
Figure 2. The results of hysteresis and acquisition of isothermal remanent magnetization experiments. (a) Day plot; (b) the IRM curves and (c) the characteristics of the low coercivity (<200 mT) section of the IRM curves. The results of the decomposition of the IRM acquisition curves of two samples are shown in two gradient acquisition plots (d and e). The multidomain (MD), single domain (SD), and superparamagnetic (SP) areas in Day plot are based on Day *et al.* (1977). The contribution of SD and MD components was determined by the SD–MD mixing curves (Dunlop 2002). The black and grey crosses on Day plot (a) and the white dotted curves on IRM aquisition plots (b and c) indicate the control sediment samples. Letters A, B1, B2 and C indicates various coercivity populations, separated by decomposition of IRM acquisition curves (please find more information in the text and Table 1).

Table 1. The results of the decomposition of IRM curves and the inflection points and Curie temperatures, identified during the thermomagnetic experiments (for additional information please see Figs 2 and 3, and the text). The background colours indicates the following separated IRM coercivity populations, classified by the similarities between the data: white—A; Light grey—B1; Medium grey—B2; Dark grey—B3; and black—C. Data written in cursive at IRM decomposition results indicate data uncertainty (i.e. very narrow DP): may influenced by measuring error, but can be related natural phenomena as well (bacterial origin). In the case of thermomagnetic experiment cursive indicates noisy curves.

Studied horizon	Sample code	Decomposition of IRM												Thermomagnetic experiments (heating curve inflection points)			
		Comp. 1				Comp. 2				Comp. 3				Infl. before bump	Peak	Small, smooth infl.	Curie temp. (T_C).
		contr. (%)	log $(B_{1/2})$	$B_{1/2}$ (mT)	DP	contr. (%)	log $(B_{1/2})$	$B_{1/2}$ (mT)	DP	contr. (%)	log $(B_{1/2})$	$B_{1/2}$ (mT)	DP				
CS1 (ash)	CS1_1 ASH	*14*	*1.05*	*11.1*	*0.03*	78	1.42	26.0	0.21	8	2.47	297.6	0.34	n.a.	(131)	325, 532	564
CS2 (bl)	CS2_1 BL	*14*	*1.03*	*10.8*	*0.03*	68	1.44	27.2	0.26	18	1.66	45.2	0.59	121	188	538	565
CS3 (ash)	CS3_ASH_2	92	1.38	23.8	0.29	8	2.34	216.7	0.41			n.a.		n.a.	*188*	*459*	*562*
CS4 (ash)	CS4_ASH_1	20	1.02	10.4	0.15	53	1.50	31.9	0.18	26	1.77	58.6	0.38	n.a.	*215*	*509*	*587*
CS5 (ash)	CS5_ASH_1	*6*	*0.90*	*8.0*	*0.03*	87	1.42	26.4	0.26	7	2.50	318.1	0.29	123	206	446	589
CS5 (bl)	CS5_10_BL_1	34	1.16	14.6	0.25	*34*	*1.67*	*46.5*	*0.08*	32	1.76	57.2	0.51	119	218	449	554
CS6 (ash)	CS6_1_ASH_1	93	1.43	26.8	0.29	7	1.94	86.1	0.44			n.a.		126	216	n.a.	580
CS7 (ash) (i)	CS7_3_ASH_1	23	0.98	9.5	0.23	64	1.47	29.7	0.23	13	2.52	328.9	0.28			n.a.	
CS7 (ash) (ii)	CS7_3_ASH_2	94	1.41	25.9	0.25	6	2.08	120.8	0.49			n.a.		130	213	477	606

which indicates significant lineation on a well determined foliation plane.

Three well defined magnetic fabric types and their less characteristic variations can be identified by the alignment of the orientation of principal susceptibilities in stereoplots (Figs 9a–g). In the first type (Figs 9a, b and c), the well gathered or intermixed κ_{max} and κ_{int} are aligned along a well (Fig. 9a) to poorly (Fig. 9c) defined

foliation plane and the relatively well grouped κ_{min} defines the foliation pole. In the case of well gathered κ_{max} of CS6 (Fig. 9a) it may indicate some force (e.g. a current) which might be responsible for the orientation of MF. In the case of the second type, represented by CS2 and CS4 (Figs 9d and e), the common feature of the MF is the intermixing of κ_{int} and κ_{min} along an axis and the well or poorly aligned κ_{max} on the foliation plane. The third type (CS3 and CS1)
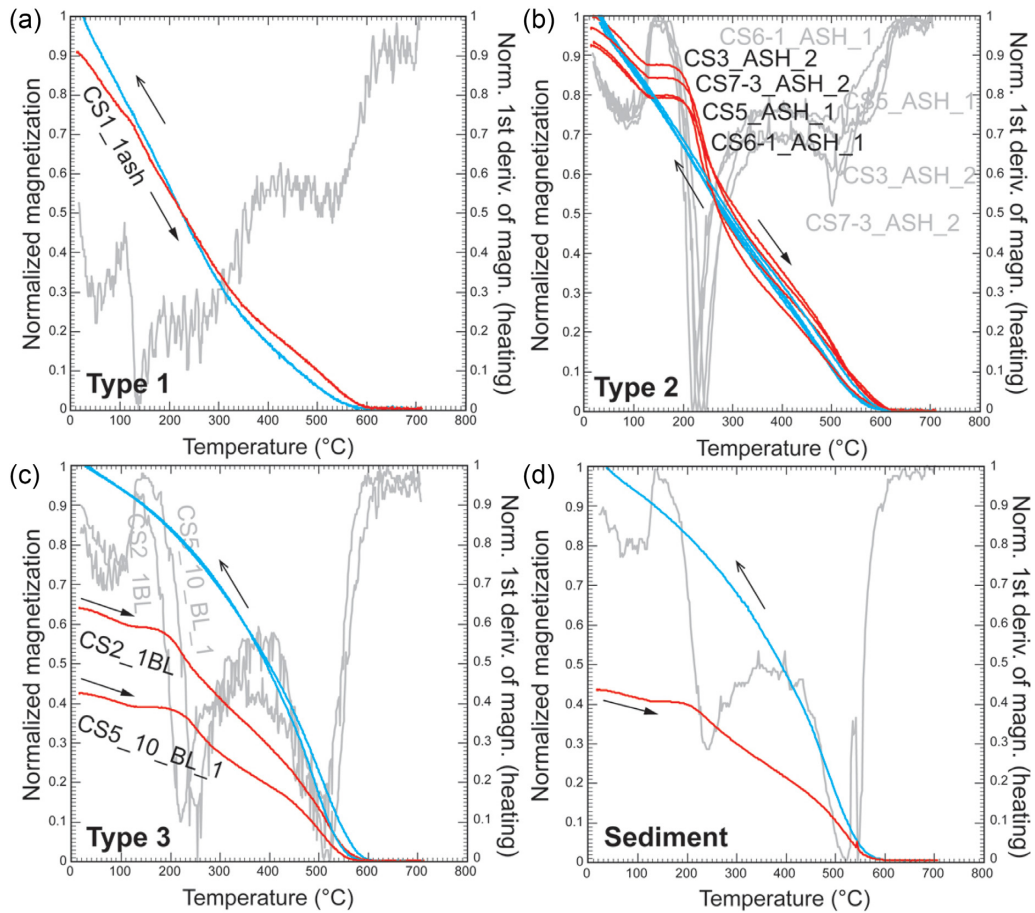
Figure 3. Various type of magnetization curves of ash samples obtained during thermomagnetic experiments (in DC fields 36 mT). Black/red (online version), solid lines—heating curve; medium grey, dashed lines/solid blue lines (online version)—cooling curves; solid light grey curves are the first derivatives of the heating curves, indicating the significant features during heating (the original data are smoothed by seven member moving average).
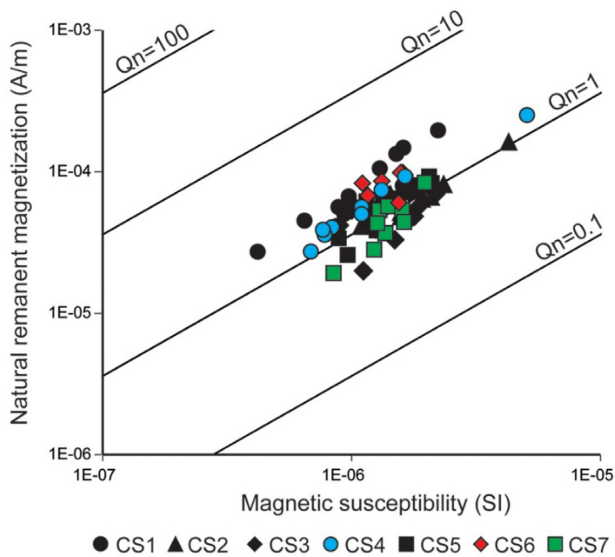

Figure 4. Natural remanent magnetization (NRM) plotted vs bulk magnetic susceptibility for every burning feature studied. Isolines of Koenigsberger ratio (Q_n) are shown. Every burning feature is distinguished according to the legend.

is defined as vertically oriented MF (compared to the theoretically horizontal foliation plane) and represented by the high inclination of κ_{max}, which gathered around the vertical. κ_{int} and κ_{min} are aligned around the quasi horizontal foliation plane (Figs 9f and g).

The common characteristics of various MF types are (i) the appearance of samples with vertically oriented fabric in all studied ash horizon (except CS2 and CS6) and (ii) the discrepancy of foliation plane from horizontal. This discrepancy is indicated by various features such as the discrepancy of κ_{min} from vertical, along with the discrepancy of κ_{max} and κ_{int} from horizontal (Figs 9a, b and c). It is also shown by the alignment of κ_{int} and κ_{min}, which instead of intermixing along an axis going through the theoretical horizontal foliation pole (Fig. 9e), represents some degree discrepancy (Fig. 9d). In the vertically oriented fabric, the dip of the foliation plane is indicated by a discrepancy of κ_{max} from vertical (Fig. 9g).

5 DISCUSSION

5.1 Magnetic mineral transformations in Middle Palaeolithic combustion structures

Following combustion, there are numerous processes that may influence the magnetic fabric and rock magnetic components of newly formed ash. The physical and chemical properties of ash, a loose,
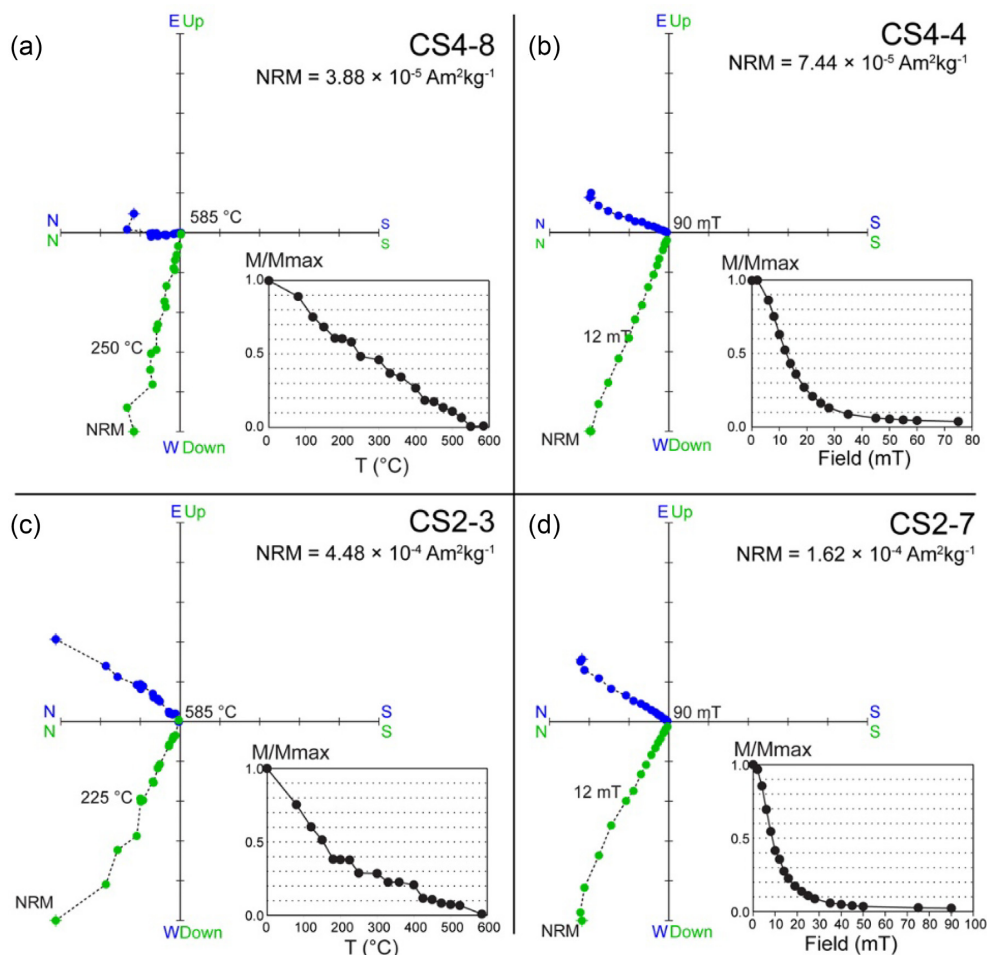
Figure 5. Representative orthogonal NRM demagnetization diagrams from the burning features studied. Green (blue) symbols represent the vertical (horizontal) projection of the vector endpoints. The sample code, NRM intensity and the normalized demagnetization spectra are also shown. (a and c) Thermal. (b and d) AF = alternating field.

Table 2. The summary of archaeomagnetic directional data. From left to right: N/N′ (number of specimens considered for the calculation of the mean direction/specimens sampled and analyzed); Dec. = Declination; Inc. = Inclination; k and α95, precision parameter and confidence limit of ChRM at the 95 per cent level (after Fisher 1953).

Burning event	N/N′	Dec. (°)	Inc (°).	k	α95 (°)
CS2	6/12	34.6	56.0	40.36	10.7
CS3	7/17	42.6	67.8	36.21	10.2
CS4	7/9	352.3	67.0	29.91	11.2
CS5	9/12	325.7	79.7	53.57	7.1
CS6	5/6	74.7	76.0	80.23	8.6
CS7	7/11	12.2	65.6	12.36	17.9
CS1	8/12	41.9	81.0	56.98	7.4

fine-grained material, may be influenced by physical and chemical alteration caused by various environmental factors such as compaction, redeposition by different surface processes and weathering (Schiegl *et al.* 1996; Bosák *et al.* 2003, Bosák & Pruner 2011; Goldberg & Sherwood 2006).

Our samples originate from seven different ash lenses within level XXIV. Previous micromorphological analyses of sediments from this level showed the presence of discrete features comprising a distinct stratigraphic sequence of black and/or reddened substrates overlain by white ash layers containing bone and charcoal inclusions, and an upper surface of very fine, pure ash (Morley 2007, p. 324). However, other parts of the sequence showed 'A chaotic mix of burnt bone, ash, limestone fragments and charcoal, presumably derived from periodic raking out of hearth deposits' (Morley 2007). Such alteration processes may have intermixed the material and caused the quasi uniform distribution of various grain sized magnetic components observed in the mixture. Such a mix of materials would show very similar magnetic grain size and coercivity characteristics. All the studied samples fell in the PSD/VS (or mixed SD and MD) region, with around 20–30 per cent of SD contributors (based on Dunlop 2002, Fig. 2a) and are characterized by soft magnetic contributors (Figs 2b and c). The narrow range of hysteresis parameters in these samples likely indicate a similar formation environments, in our case, very similar physical and chemical conditions during burning (Fig. 2a). Based on thermomagnetic curves, the main magnetic component is magnetite, which was indicated in all samples by its T_C (585 °C, Fig. 3).

The appearance of various low coercivity magnetic component is supported by the results of the decomposition of IRM curves (Figs 2d and e; Table 1). Out of the three main components (Coercivity population A, B and C), various low coercivity contributors appears most commonly as magnetic contributors. Based on the comparison the $B_{1/2}$ and DP parameters found in the literature and the parameters of the samples, the following magnetic contributors
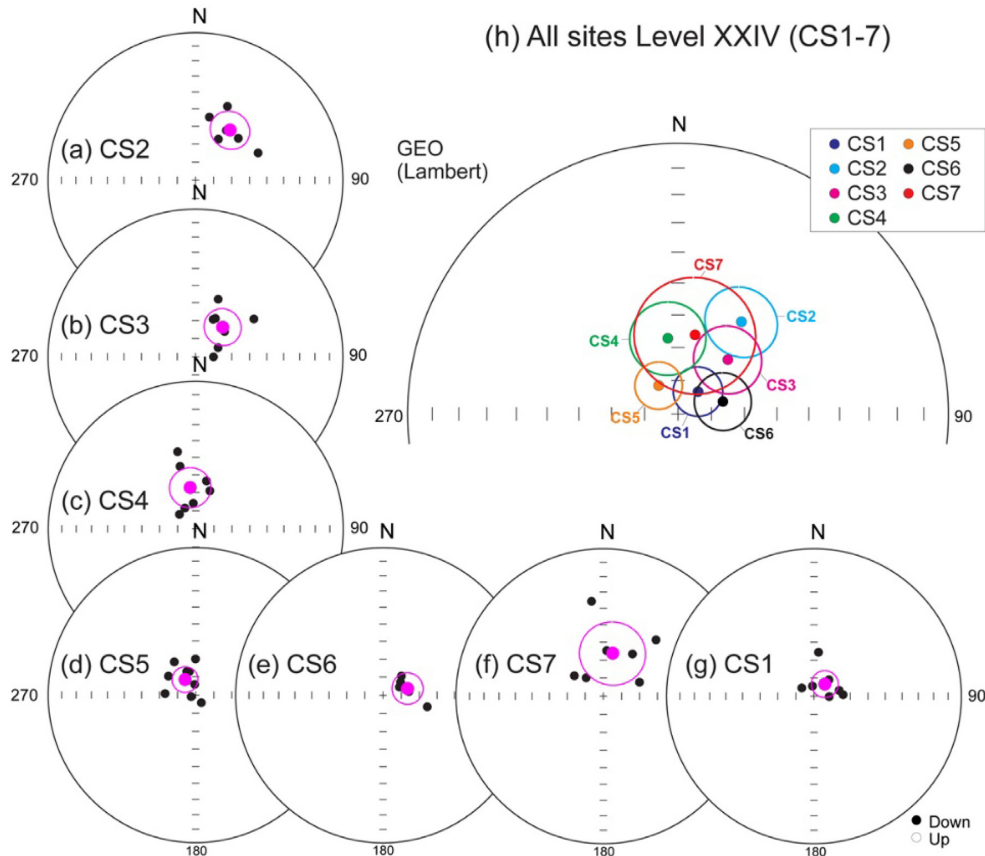
Figure 6. (a–g) Equal-area projections of all ChRM directions with the mean direction and $\alpha 95$ for every burning feature studied from level XXIV. (h) Equal-area projection with all mean directions together with their respective $\alpha 95$ distinguished by colours according to the legend. See text for explanation.

are represented by the various coercivity populations in the ash samples. Population A may represent low coercivity magnetic contributors with similar $B_{1/2}$ and DP parameters to e.g. magnetite grains below the stable SD size, magnetic minerals produced by biologically induced mineralization, pedogenic and detrital magnetite (Robertson & France 1994; Eyre 1996; Spassov *et al.* 2003; Egli 2004). The parameters of B1 coercivity population is similar to, for example synthetic SD magnetite, detrital magnetite and maghemite with a broad distribution of grain sizes, and slightly oxidized magnetite, maghemite formed by weathering (Maher 1988; Spassov *et al.* 2003; Egli 2004). As it shown above, Population A and B represent soft magnetic components (most likely magnetite) with various magnetic grain size, mainly formed during the burning and/or originated from the sediments appear in the succession (see below in detailed). The coercivity parameters of biogenic soft, non-interacting SD bacterial magnetosome component (Egli 2004) is similar to the parameters of Population B2, but the high DP in the population from ash makes its bacterial origin questionable. Based on the study of Egli (2004), DP (dispersion parameter) can be interpreted as a measure of the variability of the physical and chemical processes. In the case of simple process, for example forming of bacterial magnetite and synthetic materials, DP is close to zero, and DP is increasing by complex processes. There are only two samples where coercivity population Population B3 could be separated. $B_{1/2}$ and DP parameters of Population B3 is similar to the parameters of altered magnetite or detrital magnetite with a weathered crust of maghemite (Spassov *et al.* 2003). Determination of the $B_{1/2}$ and DP of Population C is possibly biased by the scattering (noise) of high coercivity data, which parameters possibly indicate hematite.

Compared to the very clear occurrence of the T_C of magnetite, determination of the source of the bump (Fig. 3), recognized between *ca.* 100 and 200 °C is more problematic.

Magnetization peaks such as the mentioned magnetization bump were recognized during thermomagnetic experiments on synthetic titanomagnetite powder around 100–120 °C by Day (1975), and were interpreted as a mark of the transition from SD to SP behaviour in magnetic grains close to the SSD/SP grain size boundary (Day 1975). Appearance of fine magnetic grains, including SD and SP size, related to burning is a well-known process commonly reported in archaeological burnt materials (e.g. Peters & Thompson 1999; Carrancho *et al.* 2009). Therefore, the bump may be evidence of the appearance of fine magnetic grains.

The most common mineral components in Crvena Stijena are calcite (from the natural composition of limestone and from ashes of plant residues), dolomite, quartz (from the clay and sand components of the sediments) and apatite (from bones and decomposition of organic matter, March *et al.* 2017). In addition of such common minerals, relatively high concentrations of magnetite formed during burning are found in the ash/burnt horizons (Figs 3a, b and c), similar to previous studies (e.g. McClean & Kean 1993; Carrancho *et al.* 2009, and references therein). There are numerous paths of magnetite formation during burning:

(i) Magnetite can be generated upon heating from desorption of iron-bearing mineral coatings around silicates (smectites), as shown by Hirt *et al.* (1993). Such clay minerals might be transported into the cave following surface soil erosion.
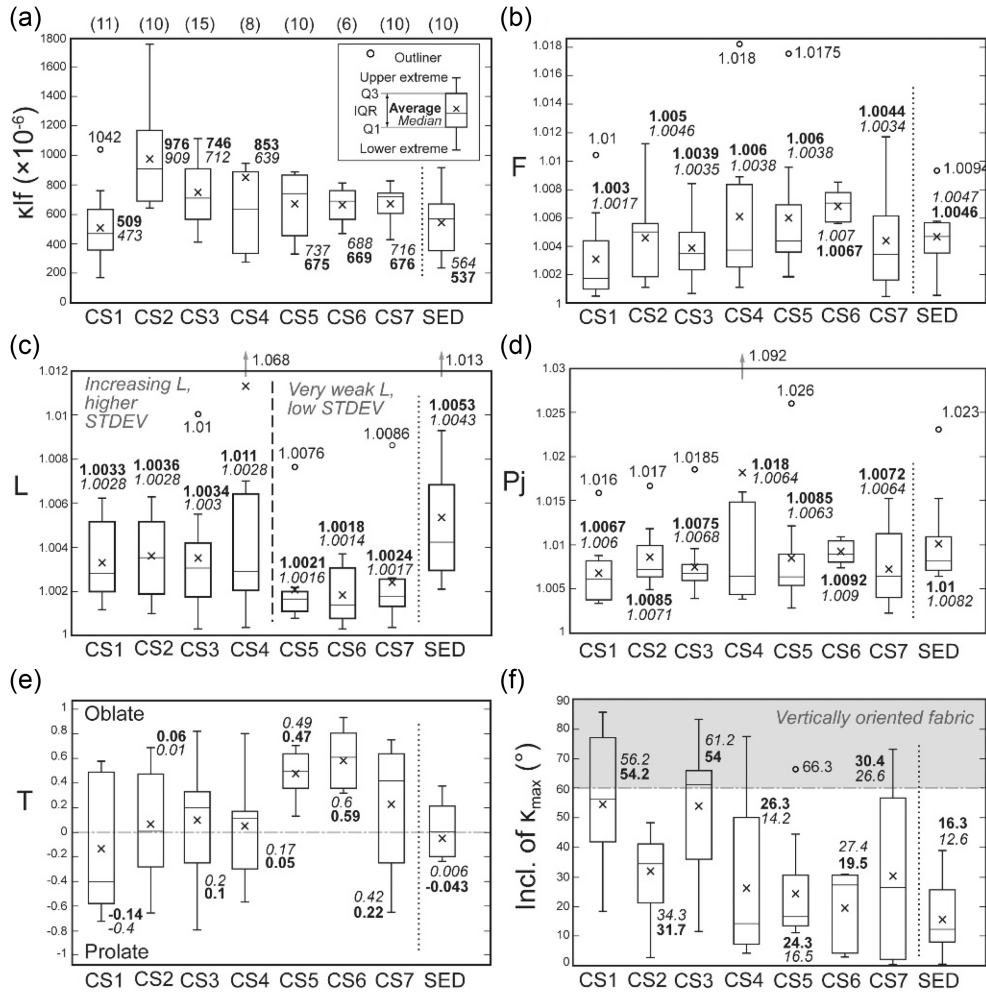
Figure 7. The box and whisker plot of the basic anisotropy parameters. Panel (a) (small figure) the boxes denote the interquartile range, whereas data falling within 1.5 times the value of the interquartile range are represented by the two T-bars (the lower and upper whiskers). Circles indicate outliers (data between 1.5–3x the interquartile range), while asterisks mark the extreme outliers (values 3x higher than the interquartile range). The black line within the box shows the median (Norušis 1993). Please find the characterization of groups marked by grey boxes (blue boxes in online version) in the text (Section 4.2). Extreme values, out of the plots are indicated by grey arrows and their values. The sample number in the studied ash horizon are indicated by the numbers in brackets below the horizon names in Fig. 4(a) and it applies for Figs 4(b) to (f). The data used during the analysis can be found in Supplementary Material 1.
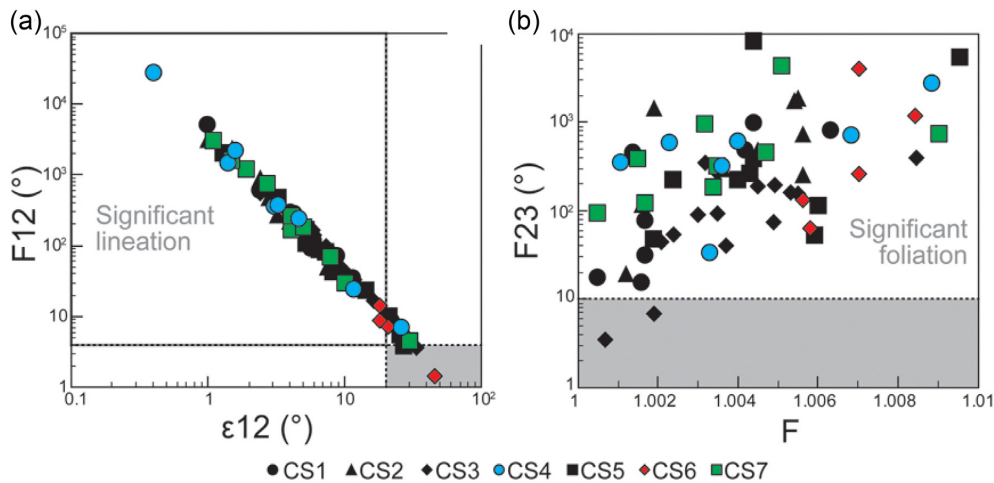

Figure 8. Samples with a.) significant lineation ($\varepsilon12 < 20$, $F12 > 4$) and b.) foliation ($F23 > 10$). The grey areas indicate only a few samples, which do not meet the criteria of Zhu *et al.* (2004), and no significant L and/or F can be found in their MF.
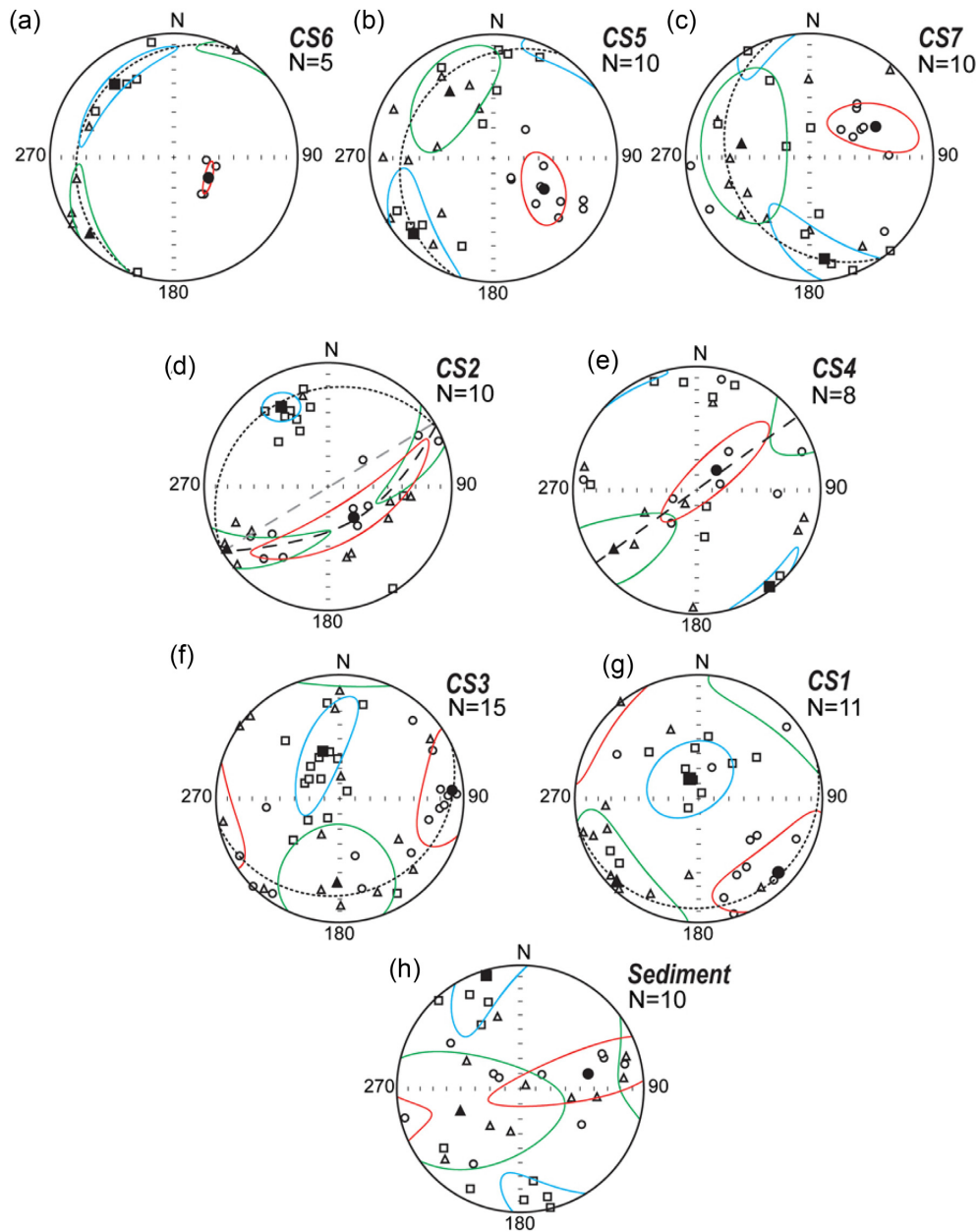
Figure 9. Characterization of the magnetic fabric of ash by the alignment of principal susceptibilities. The principal susceptibilities were plotted on stereoplots using an equal-area projection and geographical coordinate system. Solid/open squares (■/□) indicate the average maximum/maximum susceptibility, dark solid/open triangles (▲/△) represent the average intermediate/intermediate susceptibility, and solid/open circles (●/○) represent the average minimum/minimum susceptibility, respectively. The alignment and scattering of the principal susceptibilities is represented by 95 per cent confidence ellipsoids (black/blue—κ_{max}, dark grey/green—κ_{int}, and light grey/red—κ_{min} ellipsoids). Dotted lines indicate the magnetic foliation plane. Dashed lines (d, e) indicate the angle along κ_{int} and κ_{min} aligned in the case of stereoplot (d) and (e) (please find more description in the text, Sections 4.2 and 5.2).

(ii) Transformation of some paramagnetic minerals during heating (e.g. pyrite from organic material associated with combustion features and siderite originating from the shelter's geogenic carbonate) may also produce magnetite.

(iii) Another potential pathway of magnetite formation is hematite reduction, a process starting at 300–400 °C in combustion features. It probably explains the reddened substrates noted by Morley (2007, p. 324).

(iv) McClean & Kean (1993) demonstrated that wood may also carry magnetic components (phytoferritin), which may form magnetite upon heating. Magnetic enhancement by burning of plants

was also observed by Lu *et al.* (2000). Some of these processes are summarized in Carrancho *et al.* (2009).

In addition to magnetite (as main magnetic contributor), ´alternative´ interpretations of the bump (around 100–200 °C; Figs 3b and c) detailed below may explain the presence of other magnetic components, and possibly agree with the cave's sedimentary environment. Decomposition of natural siderite below 250° C and the production of, for example hematite, superparamagnetic (SP) maghemite and magnetite was described by Pan *et al.* (2002). As observed by Gallagher & Warne (1981), the decomposition temperature may decrease by the appearance of additional Mn and Mg components

in the minerals. Siderite may originate along with calcite from the limestone (e.g. ferran dolomite part; Ellwood *et al.* 1989) in which the cave was formed. It can also be formed as an authigenic mineral by precipitation from groundwater with dissolved Fe^{2+} content (Saunders & Swann 1992). The appearance of siderite may be supported by the inverse magnetic fabric observed in some samples (Figs 9c, e, f and g), similar to the fabric in dolomitic sediments in Rochette (1988). Paradoxically, the appearance of paramagnetic siderite is not strongly supported by the hysteresis curves, which show minimal para- and diamagnetic contributors in the samples.

The similarity between the rock magnetic character of some black layers (Fig. 3; Type 3, CS2 and 5) and the control sediment samples may support the appearance of post-burning alteration, mineral neoformation and/or intermixing of some ash horizons with sediments entering the rock shelter from the surface. Such processes could develop the same magnetic character as some of the sediment units in the profile (Figs 2 and 3). The fact that the control samples evidence the same bump around 150–200 °C as the ash horizons suggests that both sample types underwent the same post-burning/post-depositional alteration.

It's worth mentioning the high reversibility (coincidence between heating and cooling cycles) observed in the thermomagnetic curves in the ashes in comparison with the black layer samples. The latter are systematically irreversible generating additional secondary magnetite (Fig. 3c). Most likely, this is due to the fact that ashes reached high heating temperatures (>600–700 °C) in the past as their ferromagnetic mineralogy is not transformed when reheated again at those temperatures in the laboratory. Conversely, the subjacent black layer samples reached lower temperatures displaying a significant increase of magnetization on cooling. These results agree well with those reported in similar studies on ash and black layer samples from prehistoric fires (e.g. Carrancho *et al.* 2009, 2013, 2016b) and experimental recreations (Herrejón-Lagunilla *et al.* 2019).

5.2 Significance of MF and archaeomagnetism in the reconstruction of (post-)burning processes

A quasi uniform MF character was revealed by the basic AMS parameters of the ash horizons, which may indicate similar formation processes. These similarities in the studied ash horizons can be observed in the κlf (Fig. 7a) supported by various rock magnetic parameters (e.g. Day plot; Fig. 2a), which may indicate the similarities in mineral neoformation during burning. Burning creates the initial pyrogenic magnetic fabric, which is theoretically characterized by anisotropic, mainly oblate MF (Figs 9d and e), with quasi-horizontally (poorly) oriented minerals and also some vertically aligned component. Such characteristic anisotropy parameters and alignment of principal susceptibility axes can be found in most of the studied fabric (Figs 9a–e). Following the forming of initial pyrogenic MF, it is most likely overwritten by various processes which create various kind of magnetic fabric, characteristic for various forming environment. Those forming environments can be revealed by the analysis of the MF of ash horizons. The burning and/or the 'redeposition' of pyrogenic MF may have happened on a slight slope with some degree of inclination to horizontal (except the CS4 ash), which can be seen by the discrepancy of foliation plane from the horizontal plane (e.g. Figs 9a, b and c), similar to the fabric developed during laboratory experiments by Rees (1966). Formation on a slope can explain the scattered alignment of grains towards the slope which were initially influenced only by gravity.

The mixed quasi-horizontal and partly vertical and poor orientation can be described by the lack of a current or stress field which can strengthen the alignment of the grains (Figs 9b, c and e). Following orientation by gravity, the MFs may have been deformed due to a change in the consistency of ash (rheomorphic MF; Tarling & Hrouda 1993) and/or some low velocity slope processes (creeping, solifluction). Along with the similarities (i.e. orientation by gravity, changing of consistency, influence of forming on slope and slope processes) suggested above, some irregularities were detected, which possibly indicate alteration of the originally uniform fabric by post-burning/gravity derived processes on a slight slope (Fig. 10).

The poorly oriented grains of CS5 and CS7 (Figs 9b and c) may represent the initial pyrogenic MF, formed on slope and influenced only by gravity and some very slow velocity slope processes. In comparison, CS6 (Fig. 9a) is characterized by similar basic AMS parameters, represented by similar configuration of principal susceptibilities but with a well-defined lineation on the foliation plane (indicated by the well gathered κ_{max} orientations). As an aid for gravity and slope processes, weak/moderate energy surface processes (e.g. sheet wash) might have contributed to the formation of the better aligned fabric, which strengthened the 'slopeward' orientation of the grains (CS6; Fig. 9a). The anomalous mean archaeomagnetic direction obtained in the CS6 burning event (Dec. = 74.7°/Inc. = 76°) agrees well with these observations and points out that some type of post-burning cave process (e.g. slope processes) took place here. Additionally, the discrepancy of κ_{min} from vertical may indicate imbrication of grains, which could be related to the suggested sheet wash processes. A similar feature was identified in aeolian material and described as the result of imbrication in Nawrocki *et al.* (2006). The occurrence of water-lain sedimentation processes may be supported by the fabric of the more disturbed CS5 and CS7 horizon: infiltrating water into the loose material may (i) strengthen the influence of slope processes, triggered by the change in consistency of the ash and/or (ii) cause realignment of the grains towards the vertical plane, indicated by some (quasi-)vertical oriented samples (Figs 9b and c; Fig. 10). This interpretation is supported by analysis of carbonate values which revealed that level XXIV witnessed an increase in humid conditions (Morley 2007, p. 279), which may add further support to the idea that grains were aligned by water. These processes are coherent with the archaeomagnetic results obtained in the CS5 and CS7 combustion features. CS7 displays the worst statistical results ($k = 12$ and $\alpha95 = 17.9°$) and the lowest Q_n ratio values (mostly < 1). This indicates that this feature was physically reworked and that the record of the Earth's magnetic field direction was not very efficient here. CS5 behaves similarly to CS6 with an anomalous direction (Dec. = 325.7°/Inc. = 79.7°). Such a steep inclination is unexpected and might well be due to the aforementioned processes.

In the MF of CS2 ash, the orientation of the principal susceptibilities is well defined, showing that the magnetic contributors might have settled on a sloping surface (Fig. 9d). A similar configuration of the principal susceptibilities was reported from Mammoth Cave (Kentucky, USA) by Ellwood (1984), and interpreted as a result of flowing water along the passages. In addition, the MF of CS2 may indicate a stress field, triggered by rockfall and the impact of a huge block, observed just above the CS2 ash (Fig. 9h). A similar MF can be observed in the case of L-type tectonites (Borradaile 2001) and in rocks deformed by meteorite impacts (Yokoyama *et al.* 2012), as analogs of the impact created by a huge block falling into the ash (Fig. 10). Such a huge block of limestone is present right above the CS2 horizon (Fig. 1). Based on the size of the block, the impact
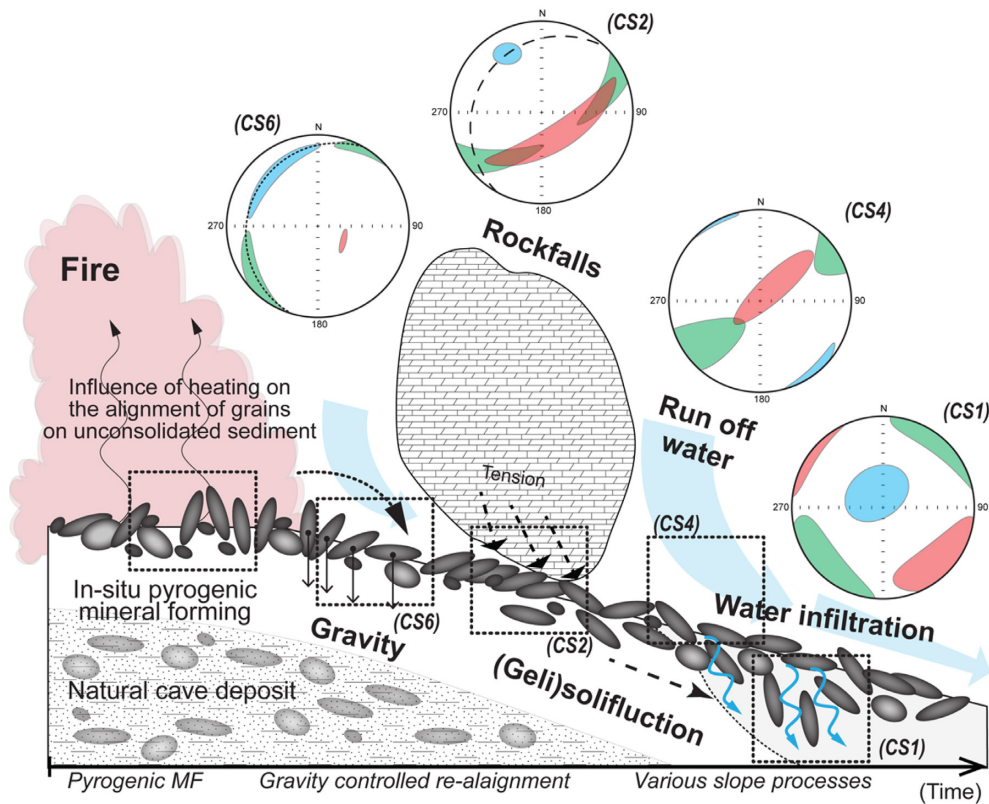
Figure 10. Combination of processes which may contribute to the development of the MF in anthropogenic burnt facies in cave successions. The ellipsoids on the stereoplots represent the theoretical alignment of the principal susceptibilities based on the 95 per cent confidence ellipsoids in the ash samples from Crvena Stijena succession (black—κ_{max}, dark grey—κ_{int} and light grey—κ_{min} ellipsoids).

might have influenced not only the magnetic fabric of the surface layer, but other layers below. However, the supposed deformation could be found only in the sediment (Fig. 9d) and the ash directly below the block, which weakens the 'rock-impact' theory. Interestingly, the boulder seems to have more effect on the MF than in the archaeomagnetic directions at least for CS2 combustion feature (the closest to the boulder). Its inclination is not particularly shallow as might have been expected (Figs 5c–d and 6a) in the case of such impact.

The principal susceptibilities of CS4 are aligned on a horizontal foliation plane, scattered and some samples show 'anomalous' vertical fabric, that is vertically oriented grains compared to the theoretically horizontal sedimentary/magnetic foliation plain, caused by various geological/pedological processes, Fig. 6e). It may represent the initial MF, suggested above.

The alignment of principal susceptibility axes may indicate inverse fabric, which can be very similar to anomalous vertical fabric. Inverse fabric can be triggered by the physical property of the magnetic grains (e.g. Parés 2015, and references therein). Inverse magnetic fabric can be formed by SD magnetic grains, but this feature is still poorly understood (Hrouda 1982; Parés 2015, and references therein). Due to the magnetic behaviour of SD grains during anisotropy of low field magnetic susceptibility measurements, orientation indicates inverse fabric. In the case of the SD grains, the susceptibility of the easy axis (the longest of an elongated grain) is the lowest (close to zero) because the magnetization is always saturated, and its orientation is indicated by the κ_{min}. That is the observed inverse MF does not indicate vertical orientation in the case of an exclusively SD fabric, but a horizontally aligned system (CS1;

Fig. 9g). Although exclusively SD material is rare in terrestrial, especially cave, sedimentary systems and none of the studied samples showed an exclusive SD character (Fig. 2a), the formation of such MF cannot be fully excluded in the case of pyrogenic processes, when the appearance of ultra-fine neoformed magnetic minerals are expected (e.g. Campbell *et al.* 1997; Jordanova *et al.* 2019). The contribution of these SP grains should generate a normal magnetic fabric.

The scattered fabric of CS3 and a better oriented CS1 (Figs 8c and f; 9f and g) ash represent 'anomalous' vertically oriented fabric. In vertically oriented magnetic fabric the alignment of κ_{max} is perpendicular to the depositional plane, that is the orientation of magnetic grains (high saturation magnetization minerals) is vertical. Vertically oriented fabrics can be formed by water infiltration and vertical migration, which re-orient the grains (e.g. Bradák-Hayashi *et al.* 2016). They indicate processes which are able to realign the grains towards vertical (and work on slopes). Such processes can be freezing and thawing along with gelifluction and (frost) creep on a slope, when tension, triggered by the expansion of frozen capillary water may vertically reorient the grains. Freezing and thawing processes and the segregation of ice lenses further lead to, for example the displacement (i.e. vertical translocation), rotation and deformation of the material (Van Vliet-Lanoë 2010), processes shown by the vertically oriented magnetic fabric of our samples (Fig. 10). Ongoing micromorphological analysis of level XXIV shows precisely these processes. The stratified combustion-derived sedimentary layers (ash lenses underlain by black layers containing burnt bone and charcoal fragments) exhibit sharp, slightly undulating contacts, moderate sorting and bedding of the sand fraction, and moderate

rotation and verticalization of some coarse particles, in addition to microstructural features typically linked with cryoturbation such as moderately developed lenticular and granular microstructures and bedded grains with silty cappings and pendants (Van Vliet-Lanoë *et al.* 1984). These characteristics also fit well with the archaeomagnetic behaviour observed in CS3 and CS1 events. The mean direction of CS3 is deflected to the east (Dec. = 42.6°/Inc. = 67.8°). In spite of the thickness of its ashes (an indicator of the thermal impact by the amount of fuel burned), its direction has been determined in a few samples and part of the ashes are somewhat irregular geometry and mixed with sediment (Fig. 1c), indicating some reworking. That also explains why almost half of these samples display Q_n ratio values <1. Combustion feature CS1 has the thickest ashes (and all Q_n ratios >1) but its mean direction is anomalous with unexpected high inclinations.

Archaeomagnetic directional data are in general coherent with the processes described by the AMS. The results obtained at combustion feature level are characterized by highly magnetic, univectorial, stable NRM diagrams along with mean directions with a reasonably acceptable statistic. However, the overall distribution is striking and can only be explained by the occurrence of some post-(burning) processes.

Some of the mean directions obtained typically exceed the expected range of secular variation for mid-latitude regions as Montenegro (between ±20° in declination and 40–70° in inclination according to similar latitudinal records as for instance the Iberian Peninsula; for examplemez-Paccard *et al.* 2006). This is particularly evident for features CS5, CS6 and CS1 and to a lesser extent CS2 and CS3, the last two with pronounced easterly mean declinations (Fig. 6 and Table 2). These observations agree well with the AMS results described above and indicate that these combustion features are not completely *in situ* from the archaeomagnetic point of view. It must be noted that the overlaps observed among some mean directions may lead to confusion as cannot be interpreted in terms of possible contemporaneity (Fig. 6h). All combustion features are exposed at different stratigraphic depths within the XXIV level being therefore asynchronous (i.e. every studied burning event happened in different geochronologic 'moment'). Due to the erratic and ribbon-like nature of the secular variation it is not surprising that an archeomagnetic direction can be repeated over time. Indeed, that is to be expected at timescales of several millennia as in this case study. The stable NRM behaviour previously described along with the moderately low scatter of the ChRM directions within sites (with the exception of CS7 site) and among them reveals that these ashes apparently recorded the Earth´s magnetic field direction at the time of their last burning. Nonetheless, considering that the mean directions are out of the expected SV range (Fig. 6h) it also indicates that they experienced some post-burning alteration process which distorted the original direction. Regardless of the post-burning alteration process (or processes) involved in these features, on the basis of the archaeomagnetic data obtained they were not very severe or at least, they do not imply a chaotic disorganization of the sediments. Otherwise, multicomponent NRM diagrams, randomly distributed mean directions and a greater statistical dispersion would be observed and that is not the case. Obviously, the obtained statistic can be improved by increasing the number of samples, but it should be noted that ashes from palaeolithic fires are difficult materials to work with. Their non-lithified nature makes them prone to move under any alteration process and they are also remarkably old materials. All these are factors to be considered.

Although the directional results would have plotted within the expected range of secular variation, the limited chronological resolution of level XXIV (between *ca*. 40–85 kya; Mercier *et al.* 2017) hampers the use of these data in geomagnetic field modelling purposes. However, they are interesting results from the archaeological point of view and particularly with regard to the identification of taphonomic processes in palaeolithic cave fires. Combined information from AMS and NRM directional data has shown that these combustion features underwent diverse post-burning mechanical alteration processes, not previously identified by macroscopic observations during the excavation and/or sampling of the site. Alteration processes in prehistoric combustion features are often identified by observations with the naked eye (e.g. irregular geometries, truncated or mixed facies, etc.). However, this study demonstrates that in caves or rock-shelters like Crvena Stijena multiple processes can affect the ashes (e.g. rotation or vertical translocation of particles by freezing and thawing processes, water percolation, slope processes, etc.), that usually go unnoted because they take place on a microscopic scale. Taking into account that archaeomagnetism and AMS deal with vectors, it is possible to identify and evaluate these processes. The main implication of demonstrating that an archaeological level has undergone some type of remobilization (including combustion features and their associated remains), is that the chrono-cultural interpretations may be compromised. Knowing the exact location where a sample (e.g. charcoal, sediment) comes from and having guarantees that it is in primary position is extremely important in geochronological studies (e.g. Mercier *et al.* 1995; Schiegl *et al.* 1996). If the alterations produce significant reworking, even archaeological remains such as bones, small lithic artefacts or palaeobotanical remains can also be translocated in the stratigraphy with obvious cultural implications. Although such a scenario is not the case at Crvena Stijena, rock-shelter, it may happen at other sites. That is why identifying these processes through the application of magnetic techniques is a helpful but still underutilized tool in geoarchaeological investigations at palaeolithic sites.

6 CONCLUSIONS

A detailed archaeomagnetic, rock magnetic and magnetic fabric study of anthropogenic ash horizons was carried out in order to better understand the formation and alteration processes of combustion features in level XXIV at Crvena Stijena.

Wood ash in anthropogenic combustion features contains neoformed magnetic minerals, which can be a good tool to assess preservation states of the ash. As indicated by the magnetic fabric and archaeomagnetic data, loose, unconsolidated wood ash from the Crvena Stijena Middle Palaeolithic fires was affected by various site formation processes. Such processes possibly include gravity derived settling of the grains, low velocity slope processes, and water infiltration-related transportation, as well as the reorientation of grains by a stress field triggered during the impact of a massive rock fall (Fig. 7). Considering previous and ongoing micromorphological data, these processes could be indicative of surface runoff and gelifluction. This study highlights the multiple, microscopic-scale alteration processes that palaeolithic combustion features can undergo. Although they hamper obtaining reliable archaeomagnetic data, valuable archaeological information can alternately be retrieved. Alteration processes in this type of material are usually identified from macroscopic field observations, so the processes described here may easily go unnoted if high-resolution techniques such as magnetic methods are not applied. The identification and evaluation of these processes has important implications for the

correct interpretation of chronological results (e.g. to ensure the exact location of samples for dating) or cultural data (possible displacements of remains in the stratigraphy), especially if significant alterations are involved. Thus, the characterization of the magnetic character of ash lenses by archaeomagnetic, rock magnetic and magnetic fabric analyses is a useful tool in the identification and evaluation of taphonomical processes in palaeolithic fires.

ACKNOWLEDGEMENTS

REFERENCES

Aldeias, V., 2017. Experimental approaches to archaeological fire features and their behavioral relevance, *Curr Anthropol.,* **58**(S16), S191–205.

Aldeias, V., Goldberg, P., Sandgathe, D., Berna, F., Dibble, H.L., McPherron, S.P., Turq, A. & Rezek, Z., 2012. Evidence for Neandertal use of fire at Roc de Marsal (France), *J. Archaeol. Sci.,* **39**(7), 2414–2423.

Baković, M., Mihailović, B., Mihailović, D., Morley, M., Vušović-lučić, Z., Whallon, R. & Woodward, J., 2009. Crvena Stijena excavations 2004–2006, preliminary report, *Eurasian Prehistory,* **6**, 3–31.

Basler, Đ., 1975a. *Crvena Stijena e Zbornik Radova*. Zajednica kulturnih ustanova, Nikšić.

Basler, Đ., 1975b. Stariji liti̱cki periodi u Crvenoj stijeni, in *Crvena Stijena e Zbornik Radova,* pp. 11–120, ed., Basler, Đ., Zajednica kulturnih ustanova, Nikšić.

Bella, P., Bosák, P., Braucher, R., Pruner, P., Hercman, H., Minár, J., Veselský, M., Holec, J. & Léanni, L., 2019. Multi-level Domica–Baradla cave system (Slovakia, Hungary): middle Pliocene–Pleistocene evolution and implications for the denudation chronology of the Western Carpathians, *Geomorphology,* **327**, 62–79.

Bondar, K. & Ridush, B., 2015. Rockmagnetic and palaeomagnetic studies of unconsolidated sediments of Bukovynka Cave (Chernivtsi region, Ukraine), *Quat. Int.,* **357**, 125–135

Borradaile, G.J., 2001. Magnetic fabrics and petrofabrics: their orientation distributions and anisotropies, *J. Struct. Geol.,* **23**, 1581–1596.

Bosák, P. & Pruner, P., 2011. Magnetic record in cave sediments: a review, in *The Earth's Magnetic Interior,* pp. 343–360, eds, Petrovský, E., Herrero-Bervera, E., Harinarayana, T. & Ivers, D., IAGA Special Sopron Book Series 1, doi:10.1007/978-94-007-0323-0̱24.

Bosák, P., Pruner, P. & Kadlec, J., 2003. Magnetostratigraphy of cave sediments: application and limits, *Stud. Geophys. Geod.,* **47**, 301–330.

Bradák-Hayashi, B., Biró, T., Horváth, E., Végh, T. & Csillag, G., 2016. New aspects of the interpretation of the loess magnetic fabric, Cérna Valley succession, Hungary, *Quat. Res.,* **86**, 348–358.

Brodar, M., 1958. Crvena stijena V e XIV stratum. Glasnik Zemaljskog muzeja Bosne i Hercegovine u Sarajevu, *Arheologija,* **13**, 43–64.

Brodar, M. 1958/59. Crvena stijena, eine neue Paläolithstation aus dem Balkan in Jugoslawien, *Quartär,* **10–11**, 227–236.

Brodar, M., 1962. Crvena Stijena 1958 i 1959, *Glas. Zemalj. muzeja Bosne i Hercegovine u Sarajevu,* **17**, 15–20.

Brodar, M., 2009. *Stara Kamena Doba V Sloveniji*. Samozal, Inštitut za arheologijo.

Campbell, A.S., Schwertmann, U. & Campbell, P.A., 1997. Formation of cubic phases on heating ferrihydrite, *Clay Miner.,* **32**, 615–622.

Carrancho, Á., Villalaín, J.J., Angelucci, D.E., Dekkers, M.J., Vallverdú, J. & Vergés, J.M., 2009. Rock-magnetic analyses as a tool to investigate archaeological fired sediments: a case study of Mirador cave (Sierra de Atapuerca, Spain), *Geophys. J. Int.,* **179**, 79–96.

Carrancho, Á. & Villalaín, J.J., 2012. Preliminary archaeomagnetic and rock-magnetic results from the Holocene fire lenses in El Mirón Cave, in *El Mirón Cave, Cantabrian Spain: The Site and its Holocene Archaeological Record,* pp. 103–118, eds, Straus, L.G. & González-Morales, R.M., New Mexico University Press.

Carrancho, Á., Villalaín, J.J., Vergés, J.M. & Vallverdú, J., 2012. Assessing postdepositional processes in archaeological cave fires through the analysis of archaeomagnetic vectors, *Quat. Int.,* **275**, 14–22.

Carrancho, Á. *et al.*, 2013. First directional European palaeosecular variation curve for the Neolithic based on archaeomagnetic data, *Earth Planet Sci Lett.,* **380**, 124–137.

Carrancho, Á., Villalaín, J.J., Vallverdú, J. & Carbonell, E., 2016a. Is it possible to identify temporal differences among combustion features in Middle Palaeolithic palimpsests? The archaeomagnetic evidence: a case study from level O at the Abric Romaní rockshelter (Capellades, Spain), *Quat. Int.,* **417**, 39–50.

Carrancho, Á., Herrejón Lagunilla, Á. & Vergés, J.M., 2016b. Three archaeomagnetic applications of archaeological interest to the study of burnt anthropogenic cave sediments, *Quat. Int.,* **414**, 244–257.

Chadima, M. & Hrouda, F., 2006. Remasoft 3.0 a user-friendly palaeomagnetic databrowser and analyzer, *Trav. Geophys.,* **27**, 20–21

Chadima, M. & Jelinek, V., 2009. *Anisoft 4.2: Anisotropy Data Browser for Windows*. Agico, Inc. https://www.agico.com/text/software/anisoft/anisoft.php.

Church, M.J., Peters, C. & Batt, C.M., 2007. Sourcing fire ash on archaeological sites in the Western and Northern Isles of Scotland, using mineral magnetism, *Geoarchaeology,* **22**, 747–774.

Day, R., 1975. Some curious thermomagnetic curves and their interpretation, *Earth Planet. Sci. Lett.,* **27**, 95–100.

Day, R.M., Fuller, M. & Schmidt, V.A., 1977. Hysteresis properties of titano-magnetites: Grain size and composition dependence, *Phys. Earth planet. Inter.,* **13**, 260–267.

Dunlop, D.J., 2002. Theory and application of the Day plot (Mrs/Ms versus Hcr/Hc) 2. Application to data for rocks, sediments, and soils, *J. geophys. Res.,* **107**(B3), 2057, doi:10.1029/2001JB000487, 2002.

Dunlop, D.J. & Özdemir, Ö., 1997. *Rock Magnetism. Fundamentals and Frontiers,* Cambridge Studies in Magnetism Series, Cambridge Univ. Press, 573p.

Ellwood, B.B., 1984. Bioturbation: minimal effects on the magnetic fabric of some natural and experimental sediments, *Earth Planet. Sci. Lett.,* **67**, 367–376.

Ellwood, B.B. *et al.*, 1989. Are the iron carbonate minerals, ankerite and ferroan dolomite, like siderite, important in paeomagnetism?, *J. geophys. Res.,* **94**, 7321–7331

Fisher, R., 1953. Dispersion on a sphere, *Proc. R. Soc., A,* **217**, 295–305.

Gallagher, P.K. & Warne, S.St.J., 1981. Thermomagnetometry and thermal decomposition of siderite, *Thermochim. Acta,* **43**, 253–267.

García Redondo, N., Carrancho, Á., Goguitchaichvili, A., Morales, J. & Palomino, Á., 2019. Comprehensive magnetic surveys of kilns for bell and tile fabrication in Castile (Spain), *J. Archaeol. Sci: Rep.,* **23**, 426–436.

Goguitchaichvili, A., García Ruiz, R., Pavón-Carrasco, F.J., Morales Contreras, J.J., Soler Arechalde, A.M. & Urrutia-Fucugauchi, J., 2018. Last three millennia Earth's Magnetic field strength in Mesoamerica and southern United States: Implications in geomagnetism and archaeology, *Phys Earth planet. Inter.,* **279**, 79–91.

Goldberg, P. & Sherwood, S.C., 2006. Deciphering human prehistory through the geoarcheological study of cave sediments, *Evol. Anthropol.,* **15,** 20–36.

Goldberg, P., Miller, C.E. & Mentzer, S.M., 2017. Recognizing fire in the Paleolithic archaeological record, *Curr. Anthropol.,* **58**(S16), S175–S190.

Gómez-Paccard, M., Chauvin, A., Lanos, P., McIntosh, G., Osete, M.L., Catanzariti, G., Ruiz-Martínez, V.C. & Núñez, J.I.(2006). First archaeomagnetic secular variation curve for the Iberian Peninsula: comparison with other data from Western Europe and with global geomagnetic field models, *Geochem. Geophys. Geosyst.,* **7,** Q12001, doi:10.1029/2006GC001476.

Gómez-Paccard, M., Rivero-Montero, M., Chauvin, A., García i Rubert, D. & Palencia-Ortas, A., 2019. Revisiting the chronology of the Early Iron Age in the north-eastern Iberian Peninsula, *Archaeol. Anthropol. Sci.,* **11,** 4755–4767, doi:10.1007/s12520-019-00812-9.

Grommé, C.S., Wright, T.L. & Peck, D.L., 1969. Magnetic properties and oxidation of Iron-Titanium oxide minerals in Alae and Makaopuhi Lava Lakes, Hawaii, *J. geophys. Res.,* 5277–5293.

Egli, R., 2004. Characterization of individual rock magnetic components by analysis of remanence curves, 1. Unmixing natural sediments, *Stud. Geophys. Geod.,* **48,** 391–446.

Eyre, JK., 1996. The application of high resolution IRM acquisition to the discrimination of remanence carriers in Chinese loess, *Stud. Geophys. Geod.,* **40,** 234–242.

Herrejón Lagunilla, Á., Carrancho, Á., Villalaín, J.J., Mallol, C. & Hernández, C.M., 2019. An experimental approach to the preservation potential of magnetic signatures in anthropogenic fires, *PLoS One,* **14**(8), e0221592, doi:10.1371/journal.pone.0221592.

Herries, A.I.R., 2009. New approaches for integrating palaeomagnetic and mineral magnetic methods to answer archaeological and geological questions on Stone Age sites, in *New Directions in Archaeological Science,* pp. 235–253, eds, Fairbairn, A., O'Connor, S. & Marwick, B., Terra Australis 28, Australian National Univ. Press, doi:10.22459/TA28.02.2009.

Heslop, D., Dekkers, M.J., Kruvier, P.P. & van Oorschot, I.H.M., 2002. Analysis of isothermal remanent magnetization acquisition curves using the expectation–maximization algorithm, *Geophys. J. Int.,* **148,** 58–64

Hirt, A.M., Banin, A. & Gehring, A.U., 1993. Thermal generation of ferromagnetic minerals from iron-enriched smectites, *Geophys. J. Int.,* **115,** 1161–1168.

Hrouda, F., 1982. Magnetic anisotropy of rocks and its application in geology and geophysics, *Geophys. Surv.,* **5,** 37–82.

Jrad, A., Quesnel, Y., Rochette, P., Jallouli, C., Khatib, S., Boukbida, H. & Demory, F., 2014. Magnetic investigations of buried Palaeohearths inside a Palaeolithic Cave (Lazaret, Nice, France), *Archaeol. Prospect.,* **21,** 87–101.

Jelinek, V., 1977. *The Statistical Theory of Measuring Anisotropy of Magnetic Susceptibility of Rocks and its Application*. Gepfyzika, 88p.

Jelinek, V., 1981. Characterization of magnetic fabric of rocks, *Tectonophysics,* **79,** 63–67.

Jordanova, N., Jordanova, D., Mokreva, A., Ishlyamski, D. & Georgieva, B., 2019. Temporal changes in magnetic signal of burnt soils – a compelling three years pilot study, *Sci. Total Environ.,* **669,** 729–738.

Kapper, K.L, Donadini, F, Mauvilly, M., Panovska, S. & Hirt, A.M., 2014a. New directional archaeomagnetic data of burned cave sediments from Switzerland and geomagnetic field variations in Central Europe, *Geophys. J. Int.,* **198**(2), 1208–1221.

Kapper, K., Anesin, D., Donadini, F., Angelucci, D., Cavulli, F., Pedrotti, A. & Hirt, A., 2014b. Linking site formation processes to magnetic properties. Rock– and archeomagnetic analysis of the combustion levels at Riparo Gaban (Italy), *J. Archaeol. Sci.,* **41,** 836–855.

Karkanas, P., Bar-Yosef, O., Goldberg, P. & Weiner, S., 2000. Diagenesis in prehistoric caves: the use of minerals that form in situ to assess the completeness of the archaeological record, *J. Archaeol. Sci.,* **27**(10), 915–929.

Kirschvink, J.L., 1980. The least-square line and plane and the analysis of paleomagnetic data, *Geophys. J. R. astr. Soc.,* **62,** 699–718.

Kruiver, P.P., Dekkers, M.J. & Heslop, D., 2001. Quantification of magnetic coercivity components by analysis of acquisition curves of isothermal remanent magnetisation, *Earth planet. Sci. Lett.,* **189,** 269–276.

Lagroix, F. & Banerjee, S.K., 2004. The regional and temporal significance of primary aeolian magnetic fabrics preserved in Alaskan loess, *Earth Planet Sci. Lett.,* **225,** 379–395.

Leonhardt, R., 2006. Analyzing rock magnetic measurements: the RockMagAnalyzer 1.0 software, *Comput. Geosci.,* **32,** 1420–1431.

Linford, N. & Platzman, E., 2004. Estimating the approximate firing temperature of burnt archaeological sediments through an unmixing algorithm applied to hysteresis data, *Phys. Earth planet. Inter.,* **147,** 197–207.

Lu, H., Liu, T., Gu, Z., Liu, B., Zhou, L., Han, J. & Wu, N., 2000. Effect of burning C3 and C4 plants on the magnetic susceptibility signal in soils, *Geophys. Res. Lett.,* **27,** 2013–2016.

Machado, J., Hernández, C.M., Mallol, C. & Galván, B.(2013). Lithic production, site formation and Middle Palaeolithic palimpsest analysis: in search of human occupation episodes at Abric del Pastor Stratigraphic Unit IV (Alicante, Spain), *J. Archaeol. Sci.,* **40**(5), 2254–2273.

Maher, B.A., 1988. Magnetic properties of some synthetic sub-micron magnetites, *Geophys. J.,* **94,** 83–96.

Mallol, C. & Henry, A., 2017. Ethnoarchaeology of Paleolithic fire: methodological considerations, *Curr. Anthropol.,* **58**(S16), S217–29.

Mallol, C., Hernández, C.M., Cabanes, D., Sistiaga, A., Machado, J., Rodríguez, Á., Pérez, L. & Galván, P., 2013. The black layer of Middle Palaeolithic combustion structures. Interpretation and archaeostratigraphic implications, *J. Archaeol. Sci.,* **40**(5), 2515–2537.

Mallol, C., Mentzer, S.M. & Miller, C.E., 2017. Combustion features, in *Archaeological Soil and Sediment Micromorphology,* pp. 299–330, eds, Nicosia, C. & Stoops, G., John Wiley & Sons Ltd.

Mallol, C. *et al.*, 2019. Fire and brief human occupations in Iberia during MIS 4: Evidence from Abric del Pastor (Alcoy, Spain), *Sci. Rep.,* **9**(1), 1–11.

March, R.J., Whallon, R. & Morley, M.W., 2017. Studying Neanderthal Fire Structures from Crvena Stijena, in *Crvena Stijena in Cultural and Ecological Context. Multidisciplinary Archaeological Research in Montenegro,* Vol. **138,** pp. 340–349, ed., Whallon, R., National Museum of Montenegro, Montenegrin Academy of Sciences and Arts, Special editions (Monographies and Studies).

McClean, R.G. & Kean, W.F., 1993. Contributions of wood ash magnetism to archaeomagnetic properties of fire pits and hearths, *Earth planet. Sci. Lett.,* **119,** 387–394.

Mentzer, SM., 2014. Microarchaeological approaches to the identification and interpretation of combustion features in prehistoric archaeological sites, *J. Archaeol. Method Theory.,* **21**(3), 616–668.

Mercier, N., Valladas, H., Joron, J.L., Schiegl, S., Bar-Yosef, O. & Weiner, S., 1995. Thermoluminescence (TL) dating and the problem of geochemical evolution of sediments. A case study: the Mousterien levels at Hayonim, *Isr. J. Chem.,* **35,** 137–142.

Mercier, N., Rink, J., Rodriquez, K., Morley, M. & Whallon, R., 2017. Absolute dating of the archaeological layers of Crvena Stijena, in *Crvena Stijena in Cultural and Ecological Context. Multidisciplinary Archaeological Research in Montenegro,* Vol. **138,** pp. 140–149, ed., Whallon, R., National Museum of Montenegro, Montenegrin Academy of Sciences and Arts, Special editions (Monographies and Studies).

Mihailović, D., Mihailović, B. & Whallon, R. 2017, Excavations of middle Paleolithic–Mesolithic layers, in *Crvena Stijena in Cultural and Ecological Context. Multidisciplinary Archaeological Research in Montenegro,* Vol. **138,** pp. 150–204, ed., Whallon, R., National Museum of Montenegro, Montenegrin Academy of Sciences and Arts, Special editions (Monographies and Studies).

Molina-Cardín, A. *et al.*, 2018. Updated Iberian archeomagnetic catalogue: new full vector paleosecular variation curve for the last three millennia, *Geochem. Geophys. Geosyst.,* **19,** 3637–3656.

Monnier, G.F., 2018. A review of infrared spectroscopy in microarchaeology: methods, applications, and recent trends, *J. Archaeol. Sci.: Rep.,* **18,** 806–823.

Morales, J., Fernández Martínez, G., Gogichaisvilli, A., Cárdenas, E. & Hernández Bernal, M.S., 2015. Archeomagnetic dating of some Pre-Columbian pottery fragments from northern Mesoamerica: implications for the chronology of central Mexico during the Epiclassic period, *J. Archaeol. Sci.: Rep.,* **4,** 32–43

Morin, E. & Soulier, M.C., 2017. The Paleolithic faunal remains from Crvena Stijena, in *Crvena Stijena in Cultural and Ecological Context. Multidisciplinary Archaeological Research in Montenegro,* vol. **138,** pp. 266–294, ed., Whallon, R., National Museum of Montenegro, Montenegrin Academy of Sciences and Arts, Special editions (Monographies and Studies).

Morley, M.W., 2007, Mediterranean Quaternary rockshelter sediment records: a multi-proxy approach to environmental reconstruction. *PhD thesis,* University of Manchester.

Morley, M.W., 2017. The geoarchaeology of Crvena Stijena: site formation processes, palaeoenvironments and hominin activity, in *Crvena Stijena in Cultural and Ecological Context. Multidisciplinary Archaeological Research in Montenegro,* Vol. **138,** pp. 82–131, ed., Whallon, R., National Museum of Montenegro, Montenegrin Academy of Sciences and Arts, Special editions (Monographies and Studies).

Morley, M. & Woodward, J., 2011. The Campanian Ignimbrite (Y5) tephra at Crvena Stijena Rockshelter, Montenegro, *Quat. Res.,* **75**(3), 683–696.

Moskowitz, B.M., 1981. Methods for estimating Curie temperatures of titanomagnetites from experimental Js-T data, *Earth Planet. Sci. Lett.,* **53,** 84–88.

Nawrocki, J., Polechońska, O., Boguckij, A. & Łanczont, M., 2006. Palaeowind directions recorded in the youngest loess in Poland and western Ukraine as derived from anisotropy of magnetic susceptibility measurements, *Boreas,* **35,** 266–271.

Norušis, M.J., 1993. *SPSS for Windows Professional Statistic Release 6.0.* SPSS Inc., p. 385.

Oliva-Urcia, B., Bartolomé, M., Moreno, A., Gil-Romera, G., Sancho, C., Muñoz, A. & Osácar, M.C., 2014. Testing the reliability of detrital cave sediments as recorders of paleomagnetic secular variations, *Catena,* **119,** 36–51.

Pan, Y., Zhu, R., Liu, Q. & Jackson, M., 2002. Low-temperature magnetic behavior related to thermal alteration of siderite, *Geophys. Res. Lett.,* **29**(23), 2087, doi:10.1029/2002GL016021, 2002.

Parés, J.M., Perez-Gonzalez, A., Arsuaga, J.L., Bermúdez de Castro, J.M., Carbonell, E. & Ortega, A., 2010. Characterizing sedimentary history of cave deposits, using archaeomagnetism and rock magnetism, Atapuerca (N Spain), *Archaeometry,* **52**(5), 882–898.

Parés, J.M., 2015. Sixty years of anisotropy of magnetic susceptibility in deformed sedimentary rocks, *Front. Earth Sci.,* **3,** 4. doi:10.3389/feart.2015.00004.

Parés, J.M. *et al.*, 2018. Chronology of the cave interior sediments at Gran Dolina archaeological site, Atapuerca (Spain), *Quat. Sci. Rev.,* **186,** 1–16.

Peters, I., Tauxe, L. & Ben-Yosef, E., 2018. Archaeomagnetic dating of pyrotechnological contexts: a case study for copper smelting sites in the Central Timna Valley, *Israel Archaeometry,* **60,** 554–570.

Peters, C. & Thompson, R., 1999. Supermagnetic enhancement, superparamagnetism, and archaeological soils, *Geoarchaeology,* **14,** 401–413.

Peters, C., Thompson, R., Harrison, A. & Church, M.J., 2002. Low temperature magnetic characterisation of fire ash residues, *Phys. Chem. Earth,* **27,** 1355–1361.

Rees, A.I., 1966. The effect of depositional slopes on the anisotropy of magnetic susceptibility of laboratory deposited sands, *J. Geol.,* **74,** 856–867.

Robertson, D.J. & France, D.E., 1994. Discrimination of remanence carrying minerals in mixtures using isothermal remanent magnetisation acquisition curves, *Phys. Earth Planet. Inter.,* **82,** 223–234.

Rochette, P., 1988. Inverse magnetic fabric in carbonate-bearinrg rocks, *Earth planet. Sci. Lett.,* **90,** 229–237.

Saunders, J.A. & Swann, C.T., 1992. Nature and origin of authigenic rhodochrosite and siderite from the Paleozoic aquifer, northeast Mississippi, U.S.A, *Appl. Geochem.,* **7,** 375–387.

Schiegl, S., Goldberg, P., Bar-Yosef, O. & Weiner, S., 1996. Ash deposits in Hayonim and Kebara Caves, Israel: macroscopic, microscopic and mineralogical observations, and their archaeological implications, *J. Archaeol. Sci.,* **23,** 763–781.

Schwarcz, H.P. & Rink, W.J., 2001. Dating methods for sediments of caves and rock shelters with examples from the Mediterranean region, *Geoarchaeology,* **16,** 355–371.

Shahack-Gross, R., Berna, F., Karkanas, P., Lemorini, C., Gopher, A. & Barkai, R., 2014. Evidence for the repeated use of a central hearth at Middle Pleistocene (300ky ago) Qesem Cave, Israel, *J. Archaeol. Sci.,* **44**(1), 12–21.

Spassov, S., Heller, F., Kretzschmar, R., Evans, M.E., Yue, L.P. & Nourgaliev, D.K., 2003. Detrital and pedogenic magnetic mineral phases in the loess/palaeosol sequence at Lingtai (Central Chinese Loess Plateau), *Phys. Earth planet. Inter.,* **140,** 255–275.

Stacey, F.D., 1967. The Koenigsberger ratio and the nature of thermoremanence in igneous rocks, *Earth planet. Sci. Lett.,* **2,** 67–68.

Tarling, D.H. & Hrouda, F., 1993. *The mAgnetic Anisotropy of Rocks,* Chapman and Hall, 218p.

Tauxe, L., 2010. *Essentials of Paleomagnetism,* Univ. California Press, 489p.

Yokoyama, E., Trindade, R.I.F., Lana, C., Souza Filho, C.R., Baratoux, D., Marangoni, Y.R. & Tohver, E., 2012. Magnetic fabric of Araguainha complex impact structure (Central Brazil): Implications for deformation mechanisms and central uplift formation, *Earth planet. Sci. Lett.,* **331–332,** 347–359

Vallverdú-Poch, J. *et al.*, 2012. Combustion structures of archaeological level O and mousterian activity areas at the Abric Romaní rockshelter (NE Iberian Peninsula), *Quat. Int.,* **247,** 313–324.

Van Vliet-Lanoë, B., Coutard, J-P. & Pissart, A., 1984. Structures caused by repeated freezing and thawing in various loamy sediments: a comparison of active, fossil and experimental data, *Earth Surf. Process. Landforms,* **9,** 553–565.

Van Vliet-Lanoë, B., 2010. Frost action, in *Interpretation of Micromorphological Features of Soils and Regoliths,* pp. 81–104, eds, Stoops, G., Marcelino, V. & Mees, F., Elsevier.

Vaquero, M. & Pastó, I., 2001. The definition of spatial units in Middle Palaeolithic sites: the hearth-related assemblages, *J. Archaeol. Sci.,* **28**(11), 1209–1220.

Weiner, S., 2010. *Microarchaeology: Beyond the Visible Archaeological Record,* Cambridge Univ. Press.

Weiner, S., Goldberg, P. & Bar-Yosef, O., 2002. Three-dimensional distribution of minerals in the sediments of Hayonim Cave, Israel: diagenetic processes and archaeological implications, *J. Archaeol. Sci.,* **29,** 1289–1308.

Whallon, R.(ed.), 2017. *Crvena Stijena in Cultural and Ecological Context. Podgorica: National Museum of Montenegro,* Montenegrin Academy of Sciences and Arts, Special editions (Monographies and Studies), Vol. **138,** p. 456.

Whallon, R. & Morin, E., 2017. Eleven years of research at Crvena Stijena: synthesis of the results, in *Crvena Stijena in Cultural and Ecological Context. Multidisciplinary Archaeological Research in Montenegro,* Vol. **138,** pp. 450–455, ed, Whallon, R., National Museum of Montenegro, Montenegrin Academy of Sciences and Arts, Special editions (Monographies and Studies).

Zeigen, C., Shaar, R., Ebert, Y. & Hovers, E., 2019. Archaeomagnetism of burnt cherts and hearths from Middle Palaeolithic Amud Cave, Israel: Tools for reconstructing site formation processes and occupation history, *J. Archaeol. Sci.,* **107,** 71–86.

Zhu, R., Liu, Q. & Jackson, M.J., 2004. Paleoenvironmental significance of the magnetic fabric of Chinese loess-paleosols since the last interglacial (< 130 ka), *Earth Planet Sci. Lett.,* **221,** 55–69.

SUPPORTING INFORMATION

Supplementary data are available at *GJI* online.

Supplementary Material 1. Additional photo documentation of the studied profile and sampling. (a) General overview of the studied section. The brackets with dashed lines indicates the focus of the

sampling in this study; the dotted lines and arrows indicate sampled horizons, (b) the sampling site of CS1 sample series, with (c) a photo documentation showing the sampling points. (d) The section of CS2, 3, 4, 5, 6 and 7 before and (f) after sampling, showing the sampling points. The marks in the field photos indicate the sampling points for further geochemical analysis.

Supplementary Material 2. The results of various magnetic studies.

Please note: Oxford University Press is not responsible for the content or functionality of any supporting materials supplied by the authors. Any queries (other than missing material) should be directed to the corresponding author for the paper.